

Paleoceanography and Paleoclimatology



RESEARCH ARTICLE

10.1029/2020PA004200

Key Points:

- Warming of interglacial surface northeast Atlantic across the mid-Pleistocene Transition
- First “100 kyr” glacial cycle preceded Marine Isotope Stage 25 (~0.95 Ma)
- Increasing Atlantic Inflow could promote ice sheet growth given pre-existence of moderately sized ice sheets

Supporting Information:

Supporting Information may be found in the online version of this article.

Correspondence to:

S. Barker,
barkers3@cf.ac.uk

Citation:

Barker, S., Zhang, X., Jonkers, L., Lordsmith, S., Conn, S., & Knorr, G. (2021). Strengthening Atlantic inflow across the mid-Pleistocene transition. *Paleoceanography and Paleoclimatology*, 36, e2020PA004200. <https://doi.org/10.1029/2020PA004200>

Received 18 DEC 2020
 Accepted 24 MAR 2021

Strengthening Atlantic Inflow Across the Mid-Pleistocene Transition

Stephen Barker¹ , Xu Zhang^{2,3}, Lukas Jonkers⁴ , Sian Lordsmith¹, Stephen Conn¹, and Gregor Knorr⁵

¹School of Earth and Environmental Sciences, Cardiff University, Cardiff, UK, ²Key Laboratory of Western China's Environmental Systems (Ministry of Education), College of Earth and Environmental Science, Lanzhou University, Lanzhou, China, ³CAS Center for Excellence in Tibetan Plateau Earth Sciences, Chinese Academy of Sciences, Beijing, China, ⁴MARUM - Center for Marine Environmental Sciences, University of Bremen, Bremen, Germany, ⁵Alfred Wegener Institute, Helmholtz Center for Polar and Marine Research, Bremerhaven, Germany

Abstract The development of larger and longer lasting northern hemisphere ice sheets during the mid-Pleistocene Transition (MPT) coincided with global cooling. Here, we show that surface waters of the north-eastern Atlantic actually warmed across this interval (~1.2–0.8 Ma), which we argue reflects an increase in the north-eastward transport of heat and moisture via the North Atlantic Current (NAC) into the Nordic Seas (the Atlantic Inflow). We suggest that simultaneous cooling and warming along the north-western and south-eastern margins (respectively) of the NAC during Marine Isotope Stage 28 (~995 ka) reflected the increasing persistence of northern ice sheets as Atlantic Inflow increased. This resulted in a diachronous shift from ~40 to ~100 kyr cyclicity across the North East (NE) Atlantic as the growing influence of northern ice sheets spread southwards; to the north-west of the NAC the first “100 kyr” cycle preceded Termination 12 (~960 ka), while on the south-eastern margin of the NAC the transition occurred ~100 kyr later. Exploratory climate model simulations suggest that increasing Atlantic Inflow at this time could have accelerated ice sheet growth because pre-existing moderately sized ice sheets allowed the positive effect of increasing precipitation to outpace melting. In addition, we propose that the dependence of post-MPT ice sheets on moisture transport via the Atlantic Inflow may ultimately contribute to their apparent vulnerability to insolation forcing once a critical size threshold is crossed and high latitude ice sheets become starved of a vital moisture source.

1. Introduction: The Mid-Pleistocene Transition and First “Missed” Interglacial: “IG 28”

The characteristic saw-tooth shape and long (~100 kyr) duration of glacial cycles within the Late Pleistocene emerged sometime around 1 million years ago during the mid-Pleistocene Transition (MPT, Clark et al., 2006; McClymont et al., 2013) (Figure 1). Prior to this, glacial cycles were largely symmetric in form with a period of ~41 kyr, more closely reflecting the influence of northern hemisphere summer insolation (Tzedakis et al., 2017). The MPT heralded not only the emergence of longer glacial cycles, but also the appearance of much larger ice sheets (Elderfield et al., 2012), despite no apparent change in orbital forcing (Figure 1). As such, it is thought to relate at least in part to the long-term cooling (believed to reflect a secular decrease in atmospheric CO₂ [Seki et al., 2010]), which gave rise to the initial development of northern hemisphere ice sheets during the Late Pliocene (Ravelo et al., 2004). However, most models (e.g., Berger & Jansen, 1994; Clark et al., 2006; McClymont et al., 2013; Willeit et al., 2019) require an additional unidirectional forcing to explain the change both in duration and intensity of glacial periods across the MPT. Importantly, any theory must account for the fact that ice sheets of the “100 kyr world” are somehow capable of surviving successive peaks in northern summer insolation, which would previously have resulted in complete deglaciation (Tzedakis et al., 2017). At the same time (and somewhat counterintuitively), it should also accommodate the apparent vulnerability of these new “super glacial” ice sheets to rather modest insolation forcing once they exceed some critical size (Raymo, 1997).

The first major phase of continental ice growth during the MPT (Figure 1) occurred within Marine Isotope Stage (MIS) 22, ~900 ka (Elderfield et al., 2012), and is thought to have been associated with a significant shift in Atlantic Ocean circulation and deep ocean carbon storage (Farmer et al., 2019; Lear et al., 2016;

© 2021. The Authors.

This is an open access article under the terms of the [Creative Commons Attribution License](https://creativecommons.org/licenses/by/4.0/), which permits use, distribution and reproduction in any medium, provided the original work is properly cited.

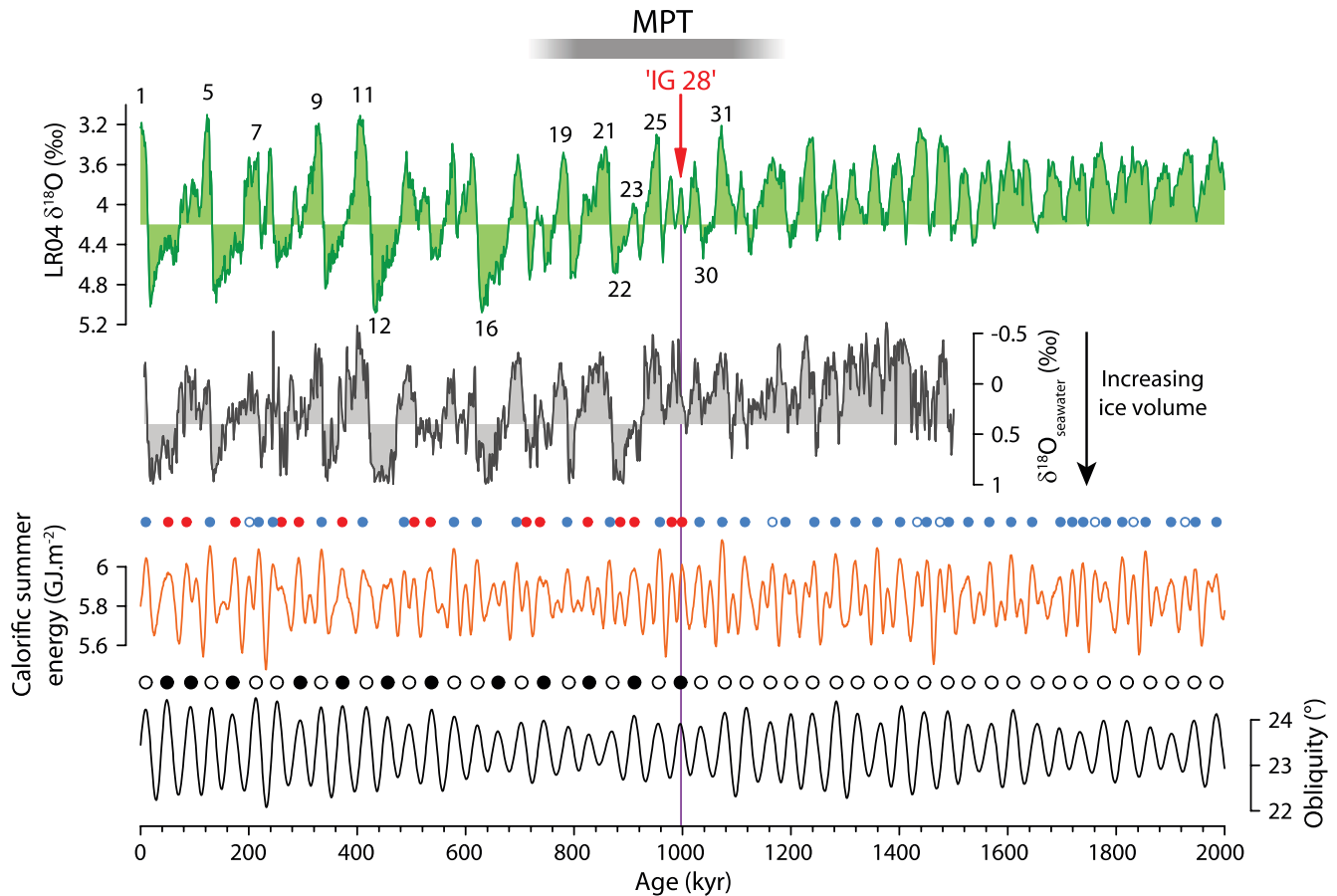


Figure 1. The first missed interglacial: “IG 28”, From top to bottom: LR04 benthic $\delta^{18}\text{O}$ stack (Lisiecki & Raymo, 2005) reveals lengthening and deepening of glacial cycles across the mid-Pleistocene Transition (MPT) (black numbers are notable Marine Isotope Stages, MIS); seawater $\delta^{18}\text{O}$ (Elderfield et al., 2012), a proxy for continental ice volume; calorific summer energy at 65°N (Tzedakis et al., 2017) (blue circles are insolation peaks that give rise to interglacials according to Tzedakis et al. (2017), red circles are peaks no longer sufficient to produce an interglacial following an increase in the threshold for deglaciation); obliquity (Berger & Loutre, 1991) (solid black circles are obliquity peaks without an associated interglacial [Tzedakis et al., 2017]). “IG 28” (purple line) represents the first missed interglacial (see text).

Pena & Goldstein, 2014). This led to the suggestion that the interval between MIS 25 and 21 could represent the first “100 kyr” glacial cycle (Pena & Goldstein, 2014). However, a recent study (Tzedakis et al., 2017) suggests that the first time an ice sheet managed to survive a peak in insolation during the MPT was significantly earlier. Tzedakis and colleagues (Tzedakis et al., 2017) developed a model to predict the occurrence of post-MPT interglacials, incorporating integrated summer insolation and a time-dependent discount applied to the level of insolation required to produce an interglacial based on when the threshold was last crossed. Crucially, the model suggests that a change in the (discounted) threshold must have occurred prior to 1 Ma in order to explain why insolation peaks after that time, which would previously have resulted in an interglacial, were no longer sufficient to do so. In other words, something in the climate system changed at or just before 1 Ma that allowed ice sheets to escape successive insolation maxima and effectively “miss” one or more interglacial.

Of particular relevance to this study are two quasi-independent predictions (implicit within the study of Tzedakis et al., 2017) of when the first “missed” interglacial (IG) may have occurred (Figure 1). First, it was shown that every peak in obliquity between 2.6 and 1 Ma (except that at 2.062 Ma) was associated with an interglacial, whereas after 1 Ma, interglacials typically occurred only with every second peak in obliquity. The first obliquity peak to miss an interglacial was ~ 995 ka (Figure 1). We note that there was a minimum in benthic $\delta^{18}\text{O}$ at that time (~ 992 – $1,002$ ka), but it does not qualify as an interglacial according to Tzedakis et al. (2017) and does not have its own MIS identifier (being counted within glacial MIS 28). For our

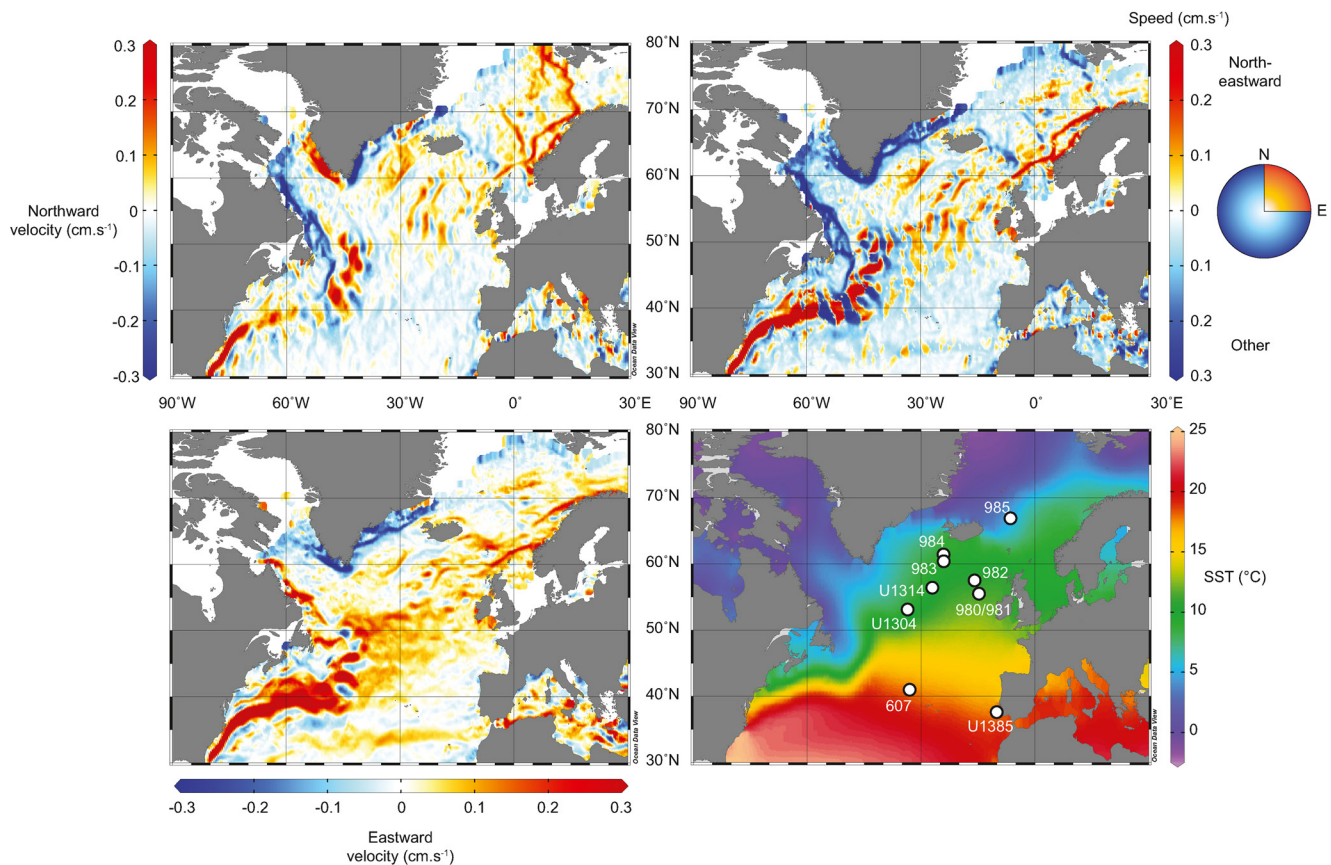
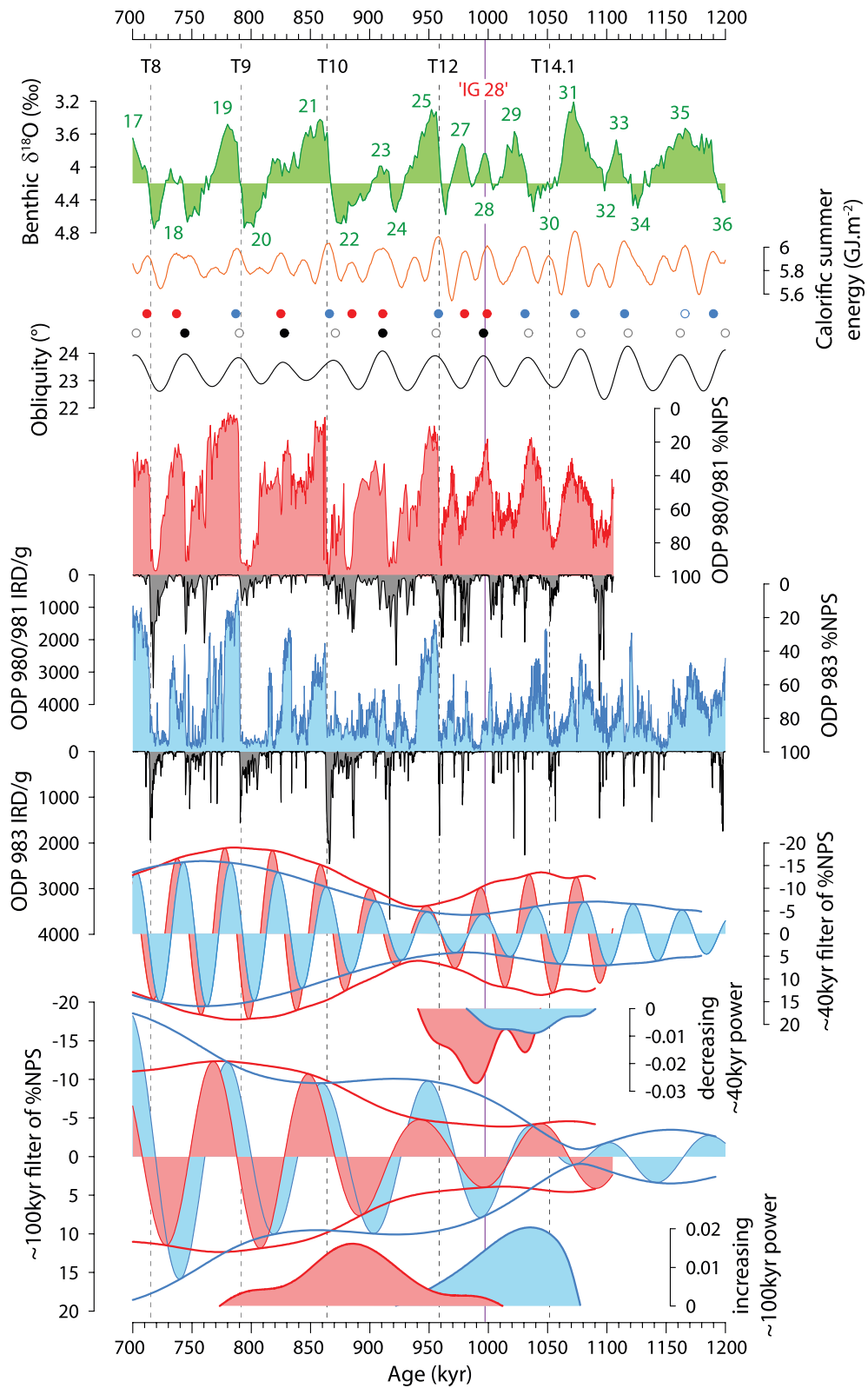


Figure 2. The North Atlantic Current (NAC) and Atlantic Inflow, Left hand panels show mean annual northward and eastward near-surface current velocities calculated from satellite-tracked drogued drifters (i.e., drifters with a -15 m sea anchor) (Lumpkin & Johnson, 2013). Upper right panel shows calculated mean annual near-surface current speed (red colors are north-eastward flow, blue colors all other directions). The Gulf Stream and its northward extension, the NAC, are depicted by the north-eastward motion of surface waters across the North Atlantic. The Atlantic Inflow represents the continuation of this transport into the Nordic Seas. Lower right panel shows core site locations referred to in main text superimposed on annual sea surface temperature (SST) (Locarnini et al., 2010). Large scale features of SST reflect surface current transport, in particular the North-eastward transport of warm surface waters into the Nordic Seas via the NAC and Atlantic Inflow systems. Maps created using Ocean Data View (Schlitzer, 2018).

purposes, we name this minimum “IG 28.” The second prediction comes from the model itself and considers the first time a peak in insolation, which would previously have given rise to an interglacial, failed to do so. That peak occurred ~ 999 ka (also coincident with IG 28; Figure 1).

The large range in age estimates for the MPT (Clark et al., 2006; McClymont et al., 2013) reflects its spatial diachronicity (i.e., changes occurred at different times in different places), making it difficult to differentiate between the various models proposed to explain it. However, most explanations center on the North Atlantic region. For example, changes in deep ocean circulation (Pena & Goldstein, 2014) (which could lower atmospheric CO_2 [Farmer et al., 2019; Lear et al., 2016]), the removal of an erodible substrate across North America (allowing the formation of larger land-based ice sheets [Clark et al., 2006]), the development of Arctic ice shelves (allowing the buildup of marine-based ice sheets [Berger & Jansen, 1994; Knies et al., 2009]) or an increase in the northward transport of heat and moisture via the North Atlantic Current (NAC) and Atlantic Inflows (Hansen & Østerhus, 2000) (the “Nordic heat pump,” [Imbrie et al., 1992] providing fuel for ice sheet growth [Berger and Jansen, 1994; Hernández Almeida et al., 2012]). Given the sensitivity of this region, we have produced high resolution (<200 years on average) records of ice rafted debris (IRD) accumulation and relative abundance of the polar affiliated planktonic foraminifer, *Neoglobobadrina pachyderma* (%NPS) from two sites (Ocean Drilling Program [ODP] Sites 981 and 983) spanning the NAC system as it enters the Nordic Seas (Figure 2). We combine these with published records (Table S1; Methods) to produce a spatiotemporal survey of the NAC as it evolved across the MPT (Figures 3–6).



2. Materials and Methods

2.1. Sample Preparation and Faunal Counts on ODP 983 and 981

For this study, we processed 2,783 samples along the splice of ODP 983 (Jansen et al., 1996) (extending previous work [Barker et al., 2015; Barker et al., 2019]) and 636 samples along the splice of ODP 981 (Jansen et al., 1996). Sediment samples were spun overnight and washed with deionized water through a 63 μm sieve before being dried at 40°C. IRD and faunal counts were made on the >150 μm fraction after splitting to yield approximately 300 entities. IRD was considered as the total number of lithogenic/terrigenous grains counted. Only left coiling specimens of *N. pachyderma* were counted and all five morphotypes of *N. pachyderma* found in recent Arctic sediments (Eynaud, 2011) were counted. Foraminiferal and IRD counts from ODP Site 980 were published previously (intermittently) back to 1 Ma (Oppo et al., 1998, 2001; Wright & Flower, 2002). Since ODP Sites 980 and 981 were recovered from the same location (Jansen et al., 1996), we are able to splice our records from Site 981 with those from Site 980 (Figure S1).

We also counted full foraminiferal assemblages for 355 samples in ODP 983, spanning several interglacial sections (Figure 5). Transfer function models (using the Modern Analogue Technique, MAT [Hutson, 1979]) were constructed using species abundance data from the ForCenS compilation (Siccha & Kucera, 2017) and annual mean sea surface temperatures from WOA1998 (Boyer et al., 1998) (use of an older data product helps to reduce the effect of global warming). RMSE (root mean squared error, defined as the square root of the average squared error between the observed and predicted values for the training set) is 1.85°C, determined using h-block cross validation to reduce the influence of spatial autocorrelation (Telford & Birks, 2009). A cut-off distance of 850 km was used, which was previously shown to be appropriate for the North Atlantic (Trachsel & Telford, 2016). We use the similarity-weighted mean temperature of the 10 best analogs to derive the estimates of past sea surface temperature. Samples with a minimum dissimilarity above the fifth percentile of the distribution of dissimilarities in the core top compilation (0.145) are considered to have poor analogs to the modern and were rejected (total 14/355). Calculations were performed in R (R_Core_Team, 2020) using the rioja package (Juggins, 2017).

2.2. Age Models for North Atlantic Cores

We place all records generated and used in this study on a common timescale for consistency and to allow direct comparison among sites on a millennial timescale. We use the timescale developed for Integrated Ocean Drilling Program (IODP) Site U1385 (Hodell et al., 2015) as a reference because this provides a target with millennial-scale resolution back to 1.5 Ma. We tuned our records from ODP Site 983 to the U1385 record of Ca/Ti (on a log scale) acquired by XRF scanning ([Hodell et al., 2015] (Figure S2). At the site of U1385, $\log(\text{Ca}/\text{Ti})$ is thought to reflect changes in the relative supply of biogenic carbonate and detrital sediment. Biogenic carbonate apparently increases during interglacial and interstadial periods and decreases during glacial and stadial periods, and therefore provides a proxy for high northern latitude millennial-scale climate variability. We limited our tuning to features in the IRD and coarse fraction records and occasional abrupt warming events (decreasing %NPS), following arguments put forward in previous studies (Austin & Hibbert, 2012; Barker et al., 2015). Hodell et al. (2015) derived several age models for U1385, but here we employ that obtained by correlating peaks in L^* (i.e., sediment color) to local summer insolation at 37°N, based on the observation of a strong precession-like signal within L^* that displays similar amplitude modulation as precession (a function of eccentricity).

We then placed records of %NPS from all sites in our survey (Table S1; except for ODP Site 985, which has too low resolution for such an exercise) onto the U1385 timescale by tuning their records to those from Site 983 (Figure S2). Where possible, we tuned the record of IRD from each site to that of Site 983 with additional

Figure 3. Diachronicity of the mid-Pleistocene Transition (MPT). From top to bottom: LR04 benthic $\delta^{18}\text{O}$ stack (Lisiecki & Raymo, 2005) (green numbers are marine isotope stage [MIS], black numbers are glacial terminations); 65°N calorific half year insolation energy (Tzedakis et al., 2017) (see Figure 1 annotation for explanation of colored symbols); obliquity (Berger and Loutre, 1991); %NPS and ice rafted debris (IRD)/g from Ocean Drilling Program (ODP) 980/981 (Wright & Flower, 2002; this study); %NPS and IRD/g from ODP 983 (Barker et al., 2019; this study); 35–45 kyr Taner filter of %NPS records with Hilbert transforms defining envelopes; rate of change of Hilbert transforms for initial decrease in ~40 kyr power (later decrease not plotted); 70–130 kyr Taner filter of %NPS records with Hilbert transforms defining envelopes; rate of change of Hilbert transforms for initial increase in ~100 kyr power (later increase not plotted). Purple line is “interglacial 28”.

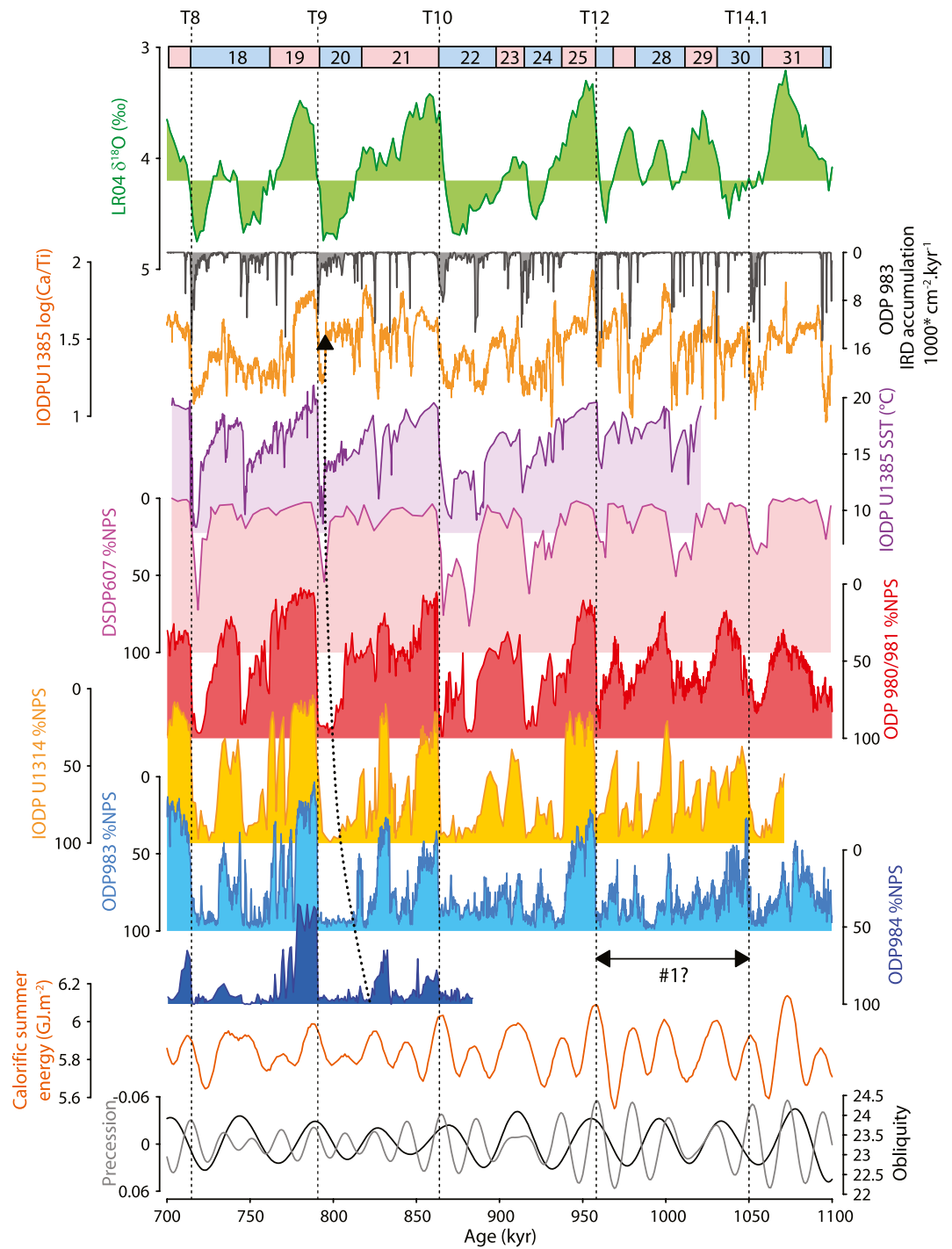
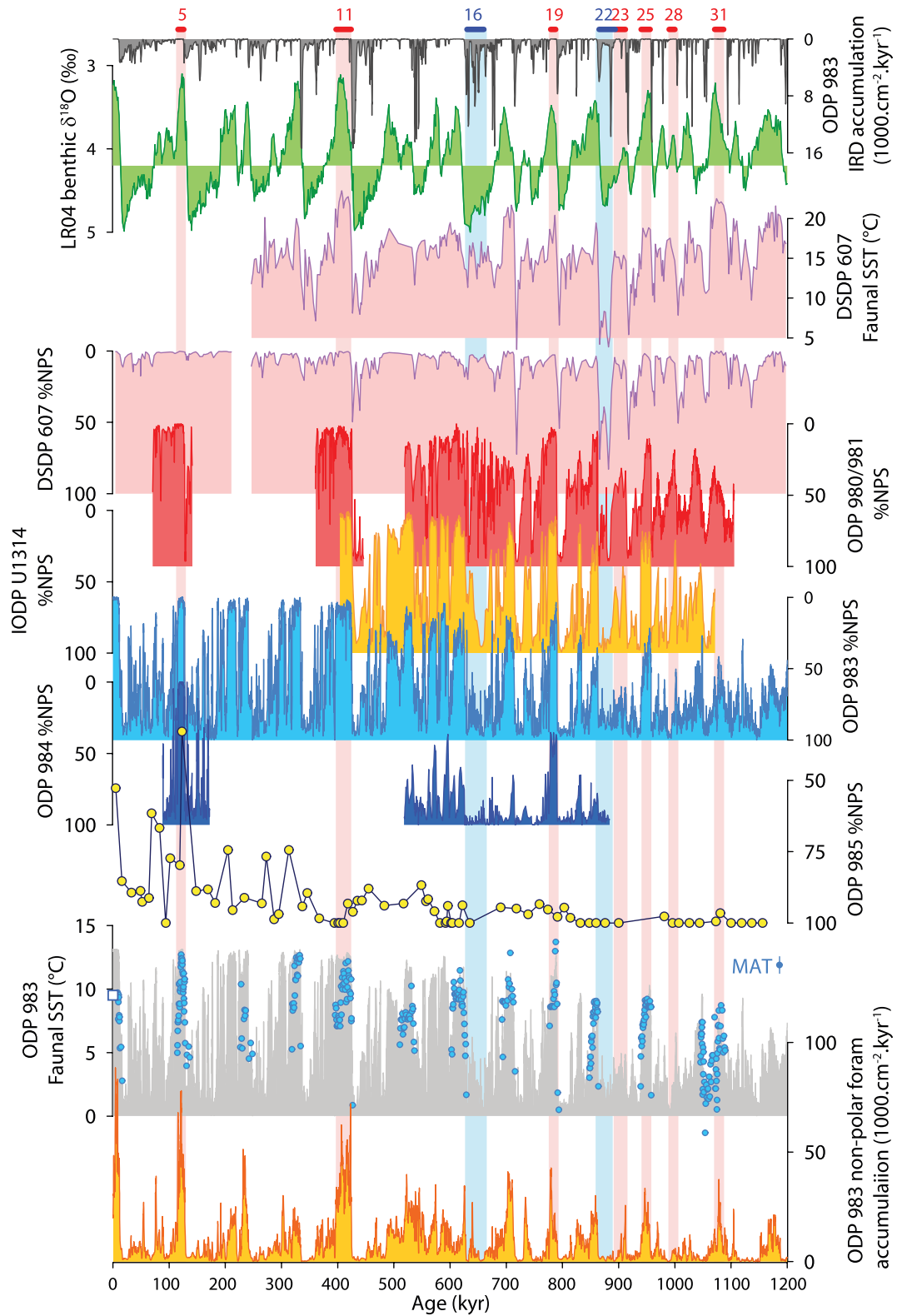


Figure 4. Emergence of the “100 kyr” world, From top to bottom: LR04 benthic $\delta^{18}\text{O}$ stack (Lisiecki & Raymo, 2005); ice rafted debris (IRD) accumulation at Ocean Drilling Program (ODP) Site 983; $\log(\text{Ca}/\text{Ti})$ (Hodell et al., 2015) and Alkenone sea surface temperature (SST) (Rodrigues et al., 2017) from Integrated Ocean Drilling Program (IODP) Site U1385; %NPS from Deep Sea Drilling Project (DSDP) 607 (Ruddiman et al., 1987), ODP 980/981 (Wright & Flower, 2002; this study), IODP U1314 (Hernández Almeida et al., 2012), ODP 983 (Barker et al., 2019; this study) and ODP 984 (Wright & Flower, 2002); integrated summer insolation at 65°N (Tzedakis et al., 2017); precession (gray) and obliquity (black) (Berger & Loutre, 1991). Pink and Blue boxes represent canonical marine isotope stages (MIS). The first “100 kyr” cycle (double-headed arrow) is bounded by T12 and T14.1. Curved dashed arrow represents south-eastward progression of the Arctic Front as glacial conditions develop.



constraints from abrupt warming events (decreases in %NPS). IRD is not recorded at Deep Sea Drilling Project (DSDP) Site 607. However, by using the age model developed by Lisiecki and Raymo (2005) for this site we note that *N. pachyderma* only becomes abundant when conditions further north are very cold and IRD is common, that is, the coldest conditions at Site 607 seem to correspond to ice rafting events further north. The same relationship is observed between the IRD record from Site 983 and the Alkenone-based sea surface temperature (SST) record from Iberian Margin Site U1385 (Rodrigues et al., 2017) (Figure S4), which were not explicitly tuned together. Accordingly, we used the record of IRD/g from ODP 983 as a tuning target for the (relatively low resolution) faunal SST record from Site 607 (Figure S2). Using this approach, we observe good agreement between the Alkenone SST records from Sites U1385 and 607 (note these records were not tuned together directly) (Figure S4). We also note that when placed on the age models derived here the records of benthic $\delta^{18}\text{O}$ from each site in our survey site do not violate their expected correlations with the LR04 benthic stack (Figure S2) (Lisiecki & Raymo, 2005).

2.3. Time series Analysis

Bandpass filtering was performed on evenly resampled (200 years) time series using a Taner filter (roll-off rate = 10^4) within the Astrochron (Meyers, 2014) Package for R (R_Core_Team, 2020). Hilbert transforms of the bandpass filtered series were also implemented using Astrochron. Rates of change of Hilbert transforms were calculated and a running mean of 10 kyr was applied before plotting (Figure 3). Wavelet transform and coherency analyses were produced using the Matlab function presented by Grinsted et al. (2004), implemented on evenly resampled (200 years) time series.

2.4. Climate Model Description

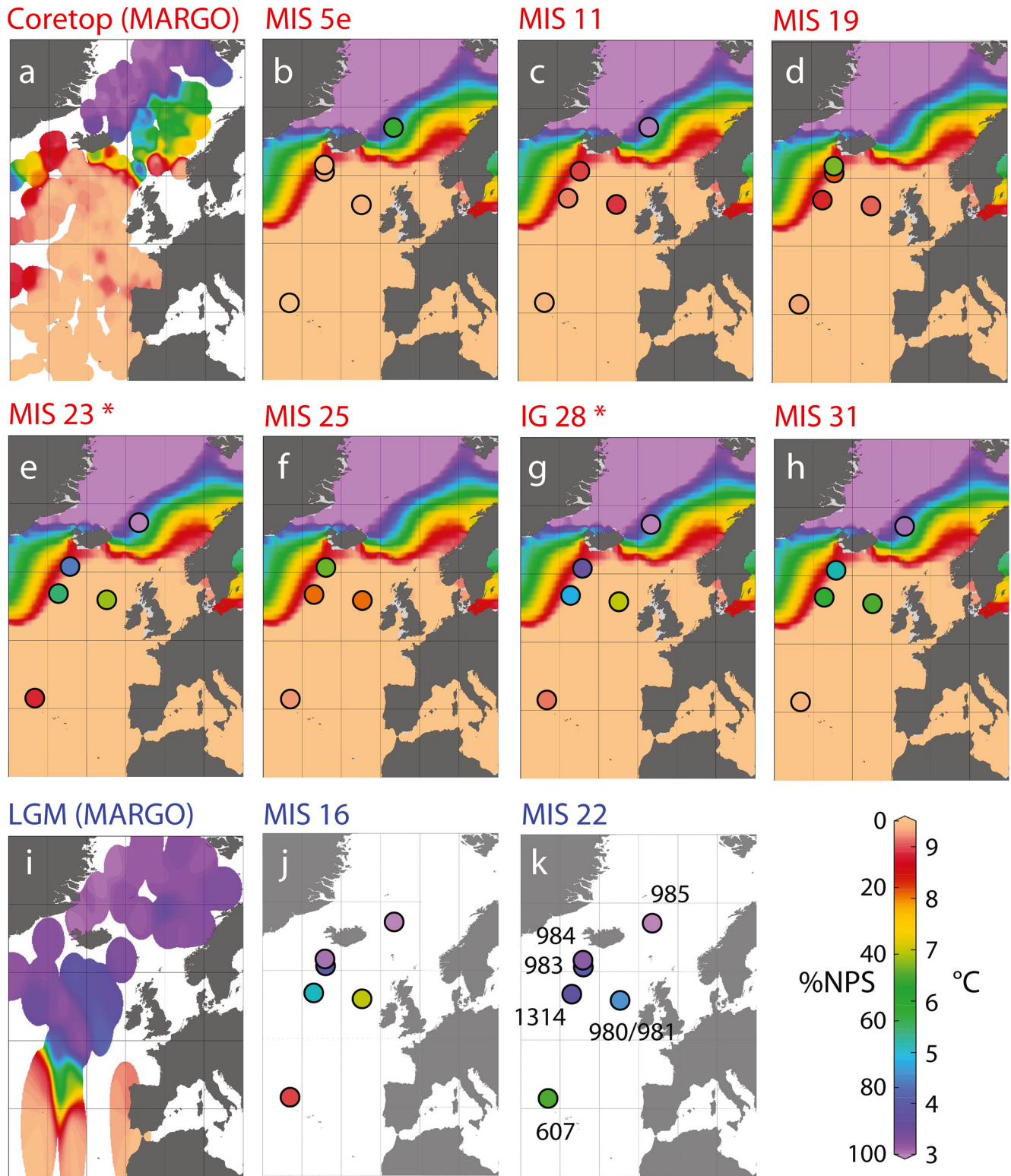
We use a comprehensive fully coupled atmosphere-ocean general circulation model (AOGCM), COSMOS (ECHAM5-JSBACH-MPI-OM) to explore the potential effects of ocean circulation on ice sheet growth. Within COSMOS the atmospheric model ECHAM5 (Roeckner et al., 2003), complemented by the land surface component JSBACH (Brovkin et al., 2009), is used at T31 resolution ($\sim 3.75^\circ$), with 19 vertical layers. The ocean model MPI-OM (Marstrand et al., 2003), including sea-ice dynamics formulated using visco-plastic rheology (Hibler III, 1979), has a resolution of GR30 ($3^\circ \times 1.8^\circ$) in the horizontal, with 40 uneven vertical layers. COSMOS has previously been used to investigate a range of paleoclimate phenomena, including the last millennium (Jungclauss et al., 2010), the Miocene warm climate (Hossain et al., 2020; Knorr & Lohmann, 2014), the Pliocene (Stepanek et al., 2020), internal variability of the climate system (Wei et al., 2012), Holocene variability (Wei & Lohmann, 2012), the Last Glacial Maximum (LGM) climate (Abelmann et al., 2015; Zhang et al., 2013) and glacial millennial-scale variability (Gong et al., 2013; Maier et al., 2018; Zhang et al., 2014, 2017). This indicates that it is capable of capturing key features of different climate states and is thus a suitable climate model for this study.

3. Results and Discussion

3.1. Diachronicity of the MPT and the First “100 kyr” Cycle

Our new records of %NPS (higher values reflect colder surface conditions) from ODP Sites 981 and 983 demonstrate the transition from ~ 41 to ~ 100 kyr periodicity across the MPT (Figure 3). Notably, the gain (decrease) of power in the ~ 100 kyr (~ 40 kyr) band at Site 983 (north-western margin of the NAC system) occurred significantly earlier than at Site 980/981 (south-eastern NAC). In particular, the gain in ~ 100 kyr

Figure 5. Evolution of North East (NE) Atlantic surface conditions since 1.2 Ma, From top to bottom: ice rafted debris (IRD) accumulation at Ocean Drilling Program (ODP) Site 983 (Barker et al., 2015, 2019; this study); LR04 benthic $\delta^{18}\text{O}$ stack (Lisiecki & Raymo, 2005); faunal sea surface temperature (SST) reconstruction and %NPS from Deep Sea Drilling Project (DSDP) 607 (Ruddiman et al., 1987); %NPS from ODP 980/981 (Oppo et al., 1998, 2001; Wright & Flower, 2002; this study), U1314 (Alonso-Garcia et al., 2011; Hernández Almeida et al., 2012), 983, 984 (Mokeddem & McManus, 2016; Mokeddem et al., 2014; Wright & Flower, 2002) and 985 (Baumann & Huber, 1999); Modern Analogue Technique (MAT) faunal SST estimates from ODP 983 (white square is modern SST, gray curve is %NPS); accumulation rate of all other species (i.e., not *N. pachyderma*) from ODP 983. Blues and pink boxes are marine isotope stage (MIS) intervals analyzed in Table S2 and shown in Figure 6.



power at Site 983 occurred during the interval spanning MIS 31–25 while at Site 980/981 the rise in ~ 100 kyr power occurred ~ 100 kyr later (across MIS 25–21). Below, we explore the reasons for this diachronicity. We begin by looking at each record individually.

At ODP Site, 980/981 we observe three typical “100kyr” glacial cycles between ~ 950 and ~ 700 ka (Figure 3). These were bounded by glacial terminations T8–T12, each of which were separated by four precession cycles. Prior to T12, warm intervals at Site 980/981 were more symmetric in appearance, and except for MIS 27, were aligned with maxima in obliquity. It is notable that although power in the obliquity band decreased just before T12, it strengthened again with the development of ~ 100 kyr periodicity after ~ 950 ka, but now the phase had shifted so that changes at Site 980/981 lagged obliquity by $\sim 90^\circ$ (Figure S3). This shift in phase reflects the more complex interactions within the coupled climate system during the Late Pleistocene (Chalk et al., 2017; Clark et al., 2006; McClymont et al., 2013; Tzedakis et al., 2017). In this case, the apparent delay in response to obliquity forcing from T12 onwards reflects the occurrence of prolonged cold periods just prior to glacial termination, while obliquity increases (Figure S3). These intervals were the new “super glacials” of the 100 kyr world, and each was followed by a much more dramatic (abrupt) deglacial warming than had previously occurred. At Site 980/981 the first of these abrupt deglacial transitions was Termination 12 (Figure 4). If glacial terminations (as defined by Broecker & van Donk, 1970) are an exclusive feature of the “100 kyr” world, this supports our contention (below) that the first 100 kyr cycle occurred prior to T12. We also note that the increasing magnitude of glacial terminations across the MPT (within our records from the North East [NE] Atlantic) was not only a function of colder glacials, but also of warmer interglacials (Figures 3–5), a point we return to in Section 3.2.

At the more northerly site (Site 983) we observe similarities and differences with Site 980/981 (Figure 3). Before ~ 1 Ma, we observe ~ 40 kyr periodicity, similar to that further south but with more pronounced millennial-scale variability presumably reflecting increased sensitivity to fluctuations in the Arctic and Polar fronts (Alonso-Garcia et al., 2011; Barker et al., 2015). Likewise, following T12 Site 983 experienced ~ 100 kyr glacial cycles similar to those at Site 980/981. The major difference between sites on the northern and southern margins of the NAC system was centered on IG 28 (Figure 3). Notably the broad obliquity-related warming seen at Site 980/981 was represented at Site 983 by a short-lived warm peak, followed by a period of pronounced cold (a similar feature is observed at Site U1314; Figure 4). The lack of a prolonged “40 kyr” warm interval during IG 28 at Site 983 directly resulted in the weakening of ~ 40 kyr periodicity and rise in ~ 100 kyr power at that location i.e., the first 100 kyr cycle at Site 983 was a result of the missed interglacial IG 28.

Our results therefore appear to confirm that the first cycle of the 100 kyr world preceded Termination 12 and that the first definitive “missed interglacial” (which we observe as a pronounced cold interval at Site 983 associated with a peak in obliquity) indeed occurred ~ 995 ka (i.e., IG 28). In addition, counting back four precession cycles from T12 (the typical duration of a Late Pleistocene glacial cycle [Cheng et al., 2016]), we observe a termination-like event (“T14.1”) $\sim 1,050$ ka within glacial MIS 30 (Figure 4). While this event cannot qualify as a canonical termination (given that benthic $\delta^{18}\text{O}$ was increasing at the time) it does bear some of the other hallmarks characteristic of Late Pleistocene glacial terminations. For example, the event comprised a pulse of IRD, followed by an abrupt decrease in %NPS (at least at Site 983). Furthermore, it directly preceded a warm (“interglacial-like”) interval at all sites in our survey (Figure 4). The event was also recorded further south on the Iberian Margin (IODP Site U1385) where the record of Ca/Ti reveals a sharp increase at this time (Figure 4), suggesting an abrupt warming (if analogous to similar events during the last 1 Myr; Figure 4 [Hodell et al., 2015; Rodrigues et al., 2017]).

We therefore hypothesize that the interval bounded by T14.1 and T12 represents the first full cycle of the ~ 100 kyr world at least within our study region. Accordingly, IG 28 appears to represent the first (definitive)

Figure 6. Spatiotemporal survey of the North East (NE) Atlantic, (a, i) %NPS from the MARGO (Margo_Project_Members, 2009) database for the Holocene (coretop) and Last Glacial Maximum (LGM) (b–h, j, k) Colored circles represent mean %NPS across selected time intervals in several NE Atlantic cores (Figure 5; Table S2). Parts (b–h) are underlain by modern annual sea surface temperature (SST) (Locarnini et al., 2010). Asterisks denote “missed interglacials”—see text. Interglacials “proper” show trend toward warmer conditions (lower %NPS) since marine isotope stage (MIS) 31. Note that relative to MIS 31 the gradient in %NPS across the North Atlantic Current (NAC) (i.e., between Site 980/981 vs. Sites 983 and 1314) increased during IG 28 as a result of warming at Site 980/981 and cooling at Sites 983 and 1314. A similar situation is observed for MIS 23 and MIS 16 relative to MIS 31. Maps were created using Ocean Data View (Schlitzer, 2018).

time that northern hemisphere ice sheets did not shrink back to their typical interglacial size despite a maximum in summer insolation that previously would have driven them to do so (Tzedakis et al., 2017). We suggest that cold conditions along the north-western margin of the NAC at this time reflected the burgeoning influence of lingering northern ice sheets, but this influence was not yet experienced by more southerly sites. In fact at the same time, we observe warmer conditions further south that were part of a longer-term trend toward warmer interglacials which (notably) commenced at or before 1.1 Ma (i.e., well before the emergence of much larger ice sheets ~ 0.9 Ma; see Section 3.2). In Sections 3.3 and 3.4, we argue that this trend reflected a strengthening of Atlantic Inflow, causing an increase in the rate of ice sheet growth and ultimately the appearance of larger ice sheets across the MPT.

We note that the T14.1 event was aligned with a peak in northern summer insolation that was a function of precession rather than obliquity (which was near to its minimum value at that time; Figure 4). Reflecting on recent conclusions about the importance of obliquity for glacial termination (Bajo et al., 2020), this observation leads us to repeat previous suggestions (e.g., Huybers, 2011) that the most parsimonious solution for the timing of glacial terminations is to call on variations in integrated summer insolation (Tzedakis et al., 2017), which combines the effects of precession and obliquity (as originally proposed [Milankovitch, 1941]), rather than contest the relative merits of one or the other.

3.2. Warming Trends Across the MPT

Most surface temperature reconstructions across the MPT suggest that this was a period of global cooling (McClymont et al., 2013) but regional warming trends have also been reported. Of particular relevance here are studies by Wright and Flower (2002) and Hernández Almeida et al. (2012) who (using results also shown here) argued for a northward migration of the (interglacial) Arctic Front (AF) since ~ 1 Ma. Our new %NPS results suggest that this trend may have begun as early as 1.2 Ma (Figure 5) and, when combined with other sites in our survey, we observe that interglacial warming during the MPT occurred right across the NAC and into the Nordic Seas (notably however equivalent records from DSDP Site 607 suggest a cooling from MIS 31 to MIS 23, implying that the warming we observe across the NE Atlantic was indeed regional; Figure 5). We observe a similar warming trend using the full foraminiferal assemblage to calculate SST at ODP Site 983 (Methods; Figure 5), in agreement with earlier findings at nearby sites (Figure S4) (Hernández Almeida et al., 2012; Wright & Flower, 2002). In accordance with our record of %NPS, we observe a trend toward warmer interglacial SSTs between MIS 31 and MIS 5 with a few warmer horizons within MIS 19 and 17 (Wright & Flower (2002) also found particularly warm temperatures during MIS 19 at Site 980; Figure S4). Our MAT temperature estimates for MIS 1 agree with modern values (Figure 5), but are significantly lower than MIS 5 by 2–3°C (RMSE = 1.85°C), which is in agreement with previous comparisons (Hoffman et al., 2017).

It has been suggested (Huber et al., 2000) that *N. pachyderma* only became fully polar affiliated at around 1.1 Ma (being only subpolar up until that time), which would imply that faunal-based records from older periods might be less reliable in terms of temperature reconstruction. On the other hand, the presence of *N. pachyderma* in the central Arctic around the time of the Olduvai geomagnetic event (Atkins, 1991) (dated to around 1.8 Ma [Kusu et al., 2016]) implies that the species was already adapted to polar conditions well before the MPT. This agrees with earlier estimates for the cold water adaption of *N. pachyderma* around 1.7 Ma (Raymo et al., 1987). Notwithstanding, it is valuable to assess the robustness of our inference of warming across the MPT.

To that end, we calculated the accumulation rate of all other species of planktonic foraminifer in ODP 983 (a quantity that is independent from %NPS; Figure 5). Although this parameter may be sensitive to other changes (e.g., primary productivity), we see a trend toward greater accumulation of nonpolar (i.e., warmer than polar) species over the last 1.2 Myr, in agreement with the trend observed in %NPS. A similar result is seen at ODP Site 985 (Figure S5) (Baumann & Huber, 1999), which is actually within the Nordic Seas (Figure 2).

Equivalent changes in the North Atlantic have also been identified in other indicator species. For example, an increase in warm diatom species after 0.84 Ma in IODP Site U1304 (Shimada et al., 2008) (Figure 2 and S5) is thought to reflect a shift from comparatively cold surface conditions (including during interglacials) prior

to 0.84 Ma, to a more modern-like situation with subtropical surface waters prevailing at Site U1304 during interglacial periods. Shimada et al. (2008) used a principle component analysis to (semi)quantify changes in surface temperature at this site (Figure S5) and although not as clear as the trend observed in records of %NPS there is a shift toward warmer (interglacial) conditions across the MPT.

However, SST reconstructions based on C37 alkenone unsaturation ratios ($U_{37}^{K'}$) from the same region as our study (and the same site in one case) do not show a warming between 1.2 and 0.9 Ma (Lawrence et al., 2009; McClymont et al., 2008) (Figure S4). On the one hand, we note good agreement between trends in $U_{37}^{K'}$ (Lawrence et al., 2010) and foraminiferal faunal-based (Ruddiman et al., 1987) SST estimates at DSDP Site 607 throughout the whole interval, with interglacial cooling between MIS 31 and MIS 25. We also note that both $U_{37}^{K'}$ and faunal SST estimates for MIS 22 at this site are significantly colder than for MIS 16, in line with %NPS records from the more southerly sites in our survey. The same is true for Iberian Margin IODP Site U1385. We also note good agreement between our faunal-based SST estimates from ODP 983 and alkenone estimates from the same core (McClymont et al., 2008) after ~1 Ma. However, the records do not agree prior to this time. In fact, the $U_{37}^{K'}$ SST estimate for MIS 31 at Site 983 is warmer than for MIS 25. A similar picture (although not as stark) is seen at ODP Site 982 (Lawrence et al., 2009) (Figure S4), which is positioned between 983 and 980/981 (Figure 2).

Differences among the various proxies used to reconstruct ocean surface temperature abound. Planktonic foraminiferal assemblages can be altered by carbonate dissolution at the sea floor (Berger, 1968), but the opposing trends we observe at ODP 983, 981 versus DSDP 607 suggest that this does not explain our observations and moreover, the carbonate content of interglacial sediments at Site 983 shows a slight decrease between 1.3 and 1 Ma (Baumann & Huber, 1999). If %CaCO₃ were taken as an indicator for dissolution we might expect %NPS to increase (rather than decrease, as we observe) as a result of its resistance to fragmentation (relative to the other common species at this site [Berger, 1970]). Alkenones can be subjected to lateral transport due to the small size of their host carrier and the even smaller alkenone molecules themselves (Ohkouchi et al., 2002) and McClymont et al. (2008) acknowledge that the accumulation of alkenones and other marine organic matter at the site of ODP 983 could reflect a combination of production in the overlying ocean and addition as well as removal of fine sediment fractions by the bottom currents, which vary as a function of deep water overflows across the Iceland-Scotland Ridge. There is also some question as to whether $U_{37}^{K'}$ SST estimates may be biased toward warmer (summer) season temperatures at higher latitudes (Prahl et al., 2010), in which case colder periods (perhaps MIS 31) could appear anomalously warm.

A possible reconciliation of this apparent discrepancy is the suggestion of increased incursion of Arctic surface waters into the NE Atlantic from ~1.15 Ma, as proposed by McClymont et al. (2008), based on the relative abundance of the C37:4 alkenone at ODP Site 983. As we discuss in Section 3.3, we believe that the warming observed across the NE Atlantic since ~1.1 Ma is a result of increasing Atlantic Inflow into the Nordic Seas. Since this inflow is just one part of the dynamic exchange of waters between the Atlantic and Arctic (and Pacific) Oceans today (Østerhus et al., 2019), it seems reasonable to suspect that an increase in Atlantic Inflow will be matched by an increase in other exchange components, including the transport of cold surface waters into the NE Atlantic from the Arctic via the East Greenland Current. If this were the case, then we might expect to find an admixture of temperature signals within this region.

In summary, given the consistency among foraminifer-based records and other proxies from cores spanning the NAC (Figure 5 and S5) and the contrasting trends observed between those and records (both foraminifer and alkenone based) from further south (DSDP Site 607; Figure S4), we suggest that the trend toward warmer interglacials across the MPT is a robust feature of the NE Atlantic. Furthermore, as stated above, the regional nature of this warming trend (on a background of global cooling) implicates a regional change in ocean dynamics, which we explore below.

3.3. Strengthening Atlantic Inflow since 1.2 Ma

It has long been held that a strong Atlantic Meridional Overturning Circulation (AMOC) is a key ingredient for the growth of large northern land-based ice sheets through its northward transport of warm, moist air (Berger & Jansen, 1994; Hebbeln et al., 1998; Ruddiman & McIntyre, 1979). Moreover, several studies (although not all; see below) have concluded that the AMOC, and particularly its north-eastern component

(the Atlantic Inflow and corresponding deep overflows [Hansen & Østerhus, 2000] aka the Nordic heat pump [Imbrie et al., 1992; Berger and Jansen, 1994]) have strengthened over the last million years or so (Baumann & Huber, 1999; Berger & Jansen, 1994; Henrich et al., 2002; Hernández Almeida et al., 2012; Poirier & Billups, 2014; M. E. Raymo et al., 2004). Our analysis provides support for this contention. The imprint of the modern NAC is apparent from maps of SST and core top %NPS (Figures 2 and 6a), which reflect the north-eastward flow of warm surface waters into the Nordic Seas. Without this flow the patterns of SST and %NPS would be more akin to those of the LGM when the polar front assumed a more zonal position (Figure 6i). Thus, the low modern values of %NPS observed at the northerly sites in our survey (Margo_Project_Members, 2009) (Figure 6a) are due to an active Nordic heat pump. By extension, we suggest (following previous studies [Hernández Almeida et al., 2012; Wright & Flower, 2002;]) that a gradual strengthening of Atlantic Inflow over the past ~1.2 Myr can explain why we observe decreasing interglacial %NPS (warming) across the NE Atlantic (implying a north-westward migration of the Arctic Front) even though global temperature trends do not share this characteristic.

Studies using a variety of approaches provide relevant information on the evolution of interglacial circulation patterns across the MPT. Records of benthic foraminiferal $\delta^{13}\text{C}$ are widely used to reconstruct circulation changes but there are severe caveats, including biological over printing and end member changes. As such, it is probably unsurprising that disagreements are common. For example, Raymo et al. (2004) constructed vertical profiles of $\delta^{13}\text{C}$ in the high-latitude North Atlantic for each glacial and interglacial period over the past 1.8 Myr. They concluded that relatively sea-ice-free conditions promoting open ocean deep convection in the modern Nordic Seas may have been limited to interglacials of the last 0.6 Myr with deep water production during earlier interglacials limited to that produced by, for example, brine rejection (i.e., they invoke a strengthening of interglacial deep water production in the Nordic Seas across the mid-Pleistocene). Based on benthic $\delta^{13}\text{C}$ records from lower latitudes (but still in the North Atlantic), Poirier and Billups (2014) also concluded that interglacial deep water production in the Nordic Seas increased across the MPT. However, Bell et al. (2015) employed benthic $\delta^{13}\text{C}$ records from the Southeast Atlantic (in combination with more northerly sites) to conclude that peak production of North Atlantic Deep Water (NADW) was reached between 2 and 1.5 Ma, becoming weaker after that time. On the other hand, one of the main conclusions drawn by Raymo et al. (2004) was that large changes in the initial $\delta^{13}\text{C}$ of northern-sourced deep water endmembers probably make inferences of past circulation changes based on benthic $\delta^{13}\text{C}$ uncertain at best.

Several studies provide alternative evidence in support of a strengthening of Atlantic Inflow and the Nordic heat pump across the MPT. For example, during the Pliocene, warm and relatively ice-free conditions in the North Atlantic region (Dowsett et al., 2010; Miller et al., 2012) (which are commonly thought to reflect a strong AMOC and enhanced Atlantic Inflow [Dowsett et al., 1992; Frenz et al., 2006; Otto-Bliesner et al., 2017; Raymo et al., 1996; Robinson et al., 2011]) were reflected in the Nordic Seas by enhanced carbonate preservation (Henrich et al., 2002). Subsequent global cooling and the initiation of major northern hemisphere glaciation in the Late Pliocene (Ravelo et al., 2004) were paralleled by a major reduction in carbonate preservation in the Nordic Seas from 2.8 to 1.2 Ma, which is thought to reflect a decrease in Atlantic Inflow (Baumann & Huber, 1999; Henrich et al., 2002). Subsequently, a shift toward higher rates of biogenic carbonate production and accumulation in the Nordic Seas since ~1.2 Ma (Figure S5) is thought to reflect increasing Atlantic Inflow since that time (Baumann & Huber, 1999; Henrich et al., 2002). This transition can be identified by a marked decrease in the contrast in carbonate sedimentation between the NE Atlantic and Nordic Seas, with the contrast becoming even less pronounced after 0.65 Ma (Baumann & Huber, 1999). Notably, this timing agrees well with the subset of studies based on benthic $\delta^{13}\text{C}$ (Raymo et al., 2004; Poirier & Billups, 2014) which argue for a strengthening of Atlantic Inflow across the MPT.

Sedimentary Nd isotopes have also been employed to reconstruct changes in the mixing between deep water endmembers across the MPT, as well as the endmembers themselves. Recent studies demonstrated a shift toward more radiogenic values of ϵ_{Nd} in the deep South Atlantic during both glacial and interglacial periods across the MPT (Farmer et al., 2019; Pena & Goldstein, 2014). The shift in glacial ϵ_{Nd} has been interpreted to reflect a reduction in the ratio of northern to southern-sourced deep water endmembers as glacials became more severe (modern northern-sourced deep waters are less radiogenic than their southern counterparts). On the other hand, the shift toward more radiogenic values of NADW during interglacials across the MPT

could be explained by an increase in the relative proportion of deep waters formed in the Nordic Seas versus the Labrador Sea (i.e., a shift in the composition of NADW). This was demonstrated in a recent modeling study (Gu et al., 2019) in which freshwater hosing across the North Atlantic produced a shift in the ϵ_{Nd} composition of NADW of $\sim 3\epsilon$ units toward less radiogenic values as the proportion of deep waters in the Nordic Seas reduced relative to those formed in the Labrador Sea (in part this reflects the much more unradiogenic ϵ_{Nd} composition of surface waters in the Labrador Sea relative to the Nordic Seas [Lambelet et al., 2016]). Recent reconstructions of the northern endmember (NADW) composition do suggest a modest shift to more radiogenic values across the MPT (-14.3 – -13.8) (Kim et al., 2018). Therefore, we suggest that the evidence from Nd isotopes is at least compatible with an increase in the interglacial formation rate of deep water production in the Nordic Seas across the MPT (and by extension an increase in Atlantic Inflow and return deep water overflows).

It should be pointed out that while we are arguing for an increase in the interglacial strength of Atlantic Inflow across the MPT (and concomitant increase in the formation and export of deep waters derived from the Nordic Seas), we cannot comment on the total rate of NADW formation, which includes a significant component derived from the Labrador Sea (Dickson & Brown, 1994). Indeed, reconstructions that point to a net decrease in the relative contributions of deep waters derived from northern versus southern sources across the MPT (e.g., Farmer et al., 2019) could be compatible with an increase in deep waters formed in the Nordic Seas if a concomitant (and potentially greater) decrease occurred in the Labrador Sea. Alternatively, an increase in southern-sourced deep water production would also appear as a decrease in the relative contribution from northern sources. A change in the relative dominance of Atlantic deep waters originating from northern versus southern sources has additional implications for climate evolution across the MPT. As mentioned, several studies suggest an intensification of southern-sourced and poorly ventilated (nutrient rich) deep waters within the glacial Atlantic basin since ~ 900 ka (Farmer et al., 2019; Pena & Goldstein, 2014), which may have contributed to the lowering of CO_2 during post-MPT glacials (Chalk et al., 2017; Lear et al., 2016). Therefore, although this change may have occurred too late to act as a trigger for the MPT, variations in deep water circulation could represent an important feedback for the intensification of glacial conditions across the MPT

3.4. Strengthening Nordic Heat Pump Promoted Larger Ice Sheets Across the MPT

Several previous studies have discussed the importance of warm surface conditions in the North Atlantic for the growth of northern ice sheets during glacial cycles of the Late Pleistocene (Alonso-Garcia et al., 2011; McManus et al., 2002; Ruddiman & McIntyre, 1979; Wright & Flower, 2002). The term “lagging warmth,” introduced by Wright and Flower (2002), refers to the tendency for locations such as ODP Site 980/981 to remain relatively warm well beyond the initial growth of northern ice sheets during the first part of a glacial cycle, as first illustrated by Ruddiman and McIntyre (1979). Alonso-Garcia et al. (2011) later used a compilation of sites to argue that northern locations experience a shorter lag than those further south and postulated a gradual south-eastward migration of the Arctic Front during glacial development, reflecting the growing influence of northern ice sheets. This time transgressive behavior of the transition to colder conditions within a glacial cycle is clearly observed in our compilation (curved dashed arrow in Figure 4), implying that warm surface water transport northwards via the NAC continues until glacial maximum conditions are attained. Our observation of a diachronous shift in the development of ~ 100 kyr periodicity during the MPT provides a longer timescale analogy to this model of glacial development. Furthermore, similar behavior is also observed on a millennial timescale during the transition from interstadial to stadial conditions across the North Atlantic (although in this case the gradual cooling is probably not due to growing ice sheets) (Barker et al., 2015).

MIS 16 (typically acknowledged as a major glaciation; Figure 1) provides a good example of the juxtaposition of (relatively) warm (to the southeast) and cold (to the northwest) surface waters across the North Atlantic while ice sheets are large (Figures 5 and 6). The record of IRD accumulation at ODP Site 983 implies a high rate of ice ablation via marine calving throughout the whole of MIS 16 (Figure 5). This presumably suggests that the rate of ice accumulation was also high throughout much of MIS 16. And yet, while conditions in the far NE Atlantic were understandably cold during that interval, we observe relatively low %NPS at ODP Site 980/981 (significantly lower than MIS 22 and even lower than MIS 31; Figures 5 and 6;

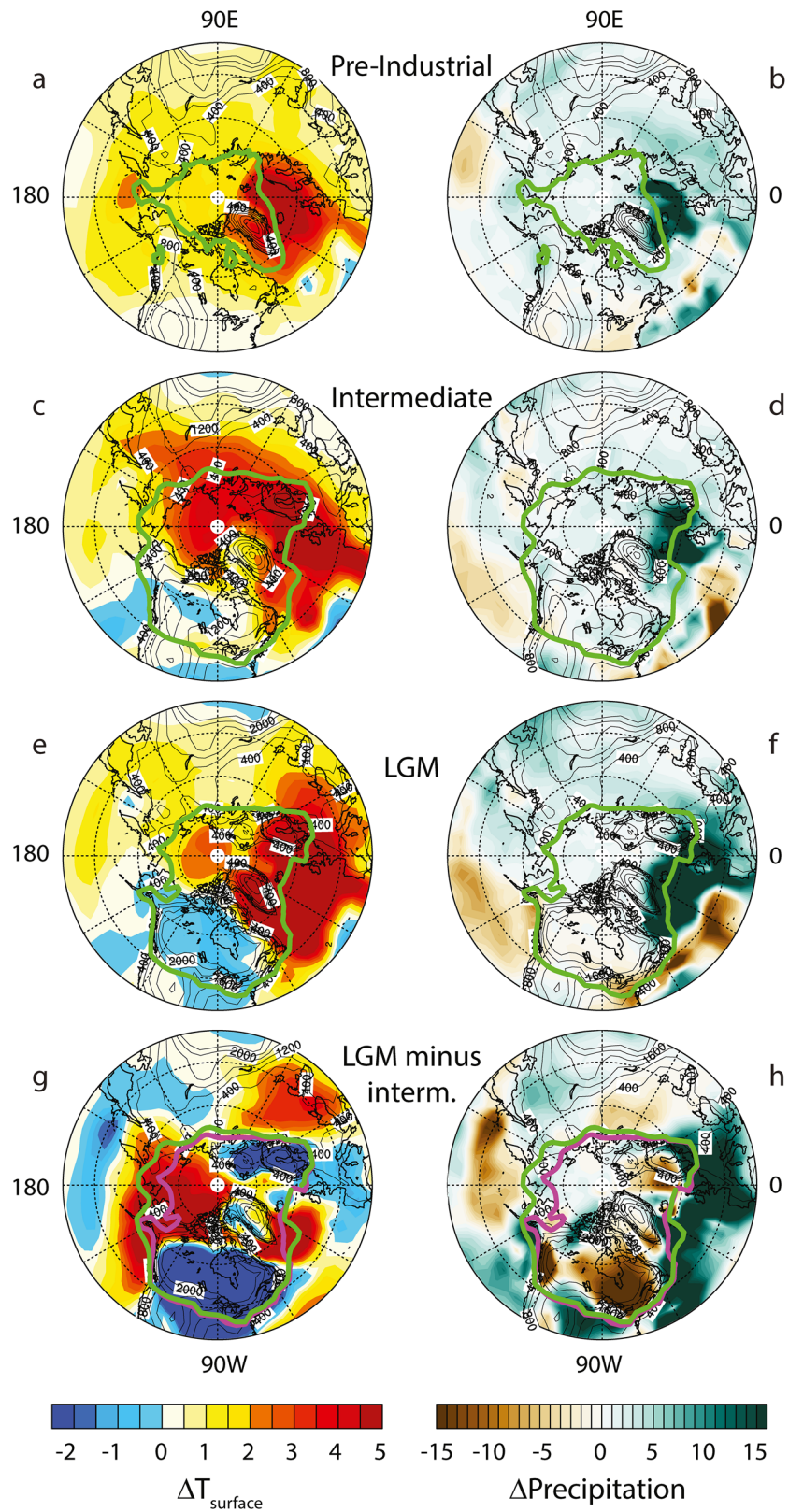
Table S2). We also note relatively warm conditions (compared to e.g., MIS 22) at more southerly sites during MIS 16 (e.g., DSDP 607 and the Iberian Margin; Figures 5 and S4). Wright and Flower (2002) noted the low concentration of *N. pachyderma* during MIS 16 at ODP Site 980. They also noted very high concentrations of *Turborotalita quinqueloba* (>40%) during the same interval, suggesting that the Arctic Front was close, but still to the northwest of the site (see their Figure 7). Accordingly, while conditions at ODP Site 980/981 could not be described as particularly warm during MIS 16 they nevertheless permit the possibility that the NAC was actively transporting surface waters north-eastwards during much of that period.

Thus, compared with MIS 31 conditions at ODP Site 980/981 were warmer (lower %NPS) during MIS 16 while further to the north and west (Sites U1314 and 983) conditions were colder (higher %NPS; Figure 6). This implies that the temperature gradient across the NAC was steeper, which we interpret to reflect the influence of large northern ice sheets superimposed on a stronger Atlantic Inflow. Critically, we see the same pattern for IG 28 and MIS 23 (lower %NPS at Site 980/981 and higher %NPS at Sites U1314 and 983 relative to MIS 31), the first and second missed interglacials according to Tzedakis et al. (2017) (Figure 6). Our results therefore imply that the growth of larger and longer lasting ice sheets across the MPT went hand in hand with strengthening of the Atlantic Inflow and support previous suggestions that the increased northward transport of warm surface waters played a direct role in the growth of larger ice sheets (Berger & Jansen, 1994; Baumann & Huber, 1999; Henrich et al., 2002; Hernández Almeida et al., 2012; Poirier & Billups, 2014).

However, other studies have concluded otherwise; that a stronger AMOC will suppress the growth of ice sheets (Bell et al., 2015). To address this issue, we ran several Earth System Model simulations (see Methods) to explore the effects of strengthening Atlantic Inflow across a range of ice sheet configurations. In our experiments, changes in Atlantic Inflow occur in response to wider AMOC perturbations that we stimulate by applying freshwater forcing across the open North Atlantic. Our experiments were designed to investigate how different boundary conditions could modulate the response of Northern Hemisphere Ice Sheet (NHIS) surface mass balance to changes in the AMOC and specifically the NAC. The surface mass balance of an ice sheet is controlled mainly by surface air temperature (SAT) and precipitation. We therefore use SAT and precipitation from our climate model experiments to qualitatively assess the effects on ice sheet mass balance. Given that the MPT spans a large range of climate sensitive parameters (including ice volume, greenhouse gases [GHG] and orbital configurations), we performed three sets of sensitivity experiments focused on different aspects.

3.4.1. Role of Pre-existing Northern Hemisphere Ice Sheets

We conducted three pairs of sensitivity experiments to investigate how pre-existing NHIS can modulate the response of ice-sheet surface mass balance to a change in Atlantic Inflow, respectively under Preindustrial (PI), 40% LGM NHIS (IntICE) (Zhang et al., 2014) and full LGM conditions (Table S3). In the 40% LGM scenario NHIS are set to 40% of their LGM size while Antarctica is set to its LGM size (as described by Zhang et al., 2014). Global ice volume is therefore equivalent to -62 m. These values are within the range of previous estimates for pre-MPT ice volumes, which suggest that northern ice sheets may have grown to >50% of their LGM size prior to 1 Ma (Bintanja & Van de Wal, 2008), while total ice volume reached -50 – -80 m SLE with respect to modern (Bintanja & Van de Wal, 2008; Elderfield et al., 2012). To achieve comparable changes in North Atlantic currents among different experiments, we conducted North Atlantic freshwater hosing experiments on each of the basic states to stimulate changes (in this case a weakening) in the AMOC and reduction in Atlantic Inflow. Note that in contrast to the PI and IntICE experiments, which were hosed with 0.15 Sv, we applied a freshwater flux of 0.2 Sv to the LGM experiment to maintain the AMOC in a weak state because a weak-to-strong AMOC transition can be triggered when atmospheric CO_2 reaches ~ 220 ppm under LGM conditions even with a persistent North Atlantic hosing of 0.15 Sv (Zhang et al., 2017). Note that this does not affect comparisons between the “strong AMOC” mode of the various scenarios (e.g., Figures 7g and 7h). GHG in these experiments were uniformly set to an intermediate level (atmospheric $\text{CO}_2 = 220$ ppmv) to account for slightly higher pre-MPT glacial values of CO_2 (Chalk et al., 2017; Hönlisch et al., 2009). This setup ensures that the simulated response of ice sheet surface mass balance is mainly a function of pre-existing NHIS configurations (as opposed to atmospheric CO_2). Each hosing run was integrated for 800 years to ensure that the perturbed climate was close to quasi-equilibrium and the final 100 years was integrated to represent the corresponding climatology (Figure S6). Note that we



do not have a quantitative estimate for how much the Atlantic Inflow might actually have varied over the period of interest and as such our results should be interpreted qualitatively.

For all ice-sheet configurations we observe a shift to warmer temperatures and increased precipitation across the North Atlantic region and beyond as the AMOC and Atlantic Inflow strengthen (Figure 7) but critically the net effect on ice sheet growth will depend on their initial size. Starting with ice sheets similar to their modern (pre-industrial) size, warming occurs over all regions of potential ice sheet formation as the AMOC and Atlantic Inflow strengthen. This will potentially inhibit ice sheet growth except over Greenland, where surface temperatures remain below zero (Figure 7a). However, when northern ice sheets are at an intermediate size the growth rate of all northern hemisphere ice sheets will potentially increase as Atlantic Inflow strengthens. This is because the 0° summer surface (2 m) temperature contour remains south of the major ice sheets while precipitation increases over them (at least in the Eurasian sector; Figures 7c and 7d). A similar effect is seen for large (LGM) ice sheets (Figures 7e and 7f) but in this case the NAC is more zonal in nature (in agreement with reconstructions for the LGM and previous glacial maxima [Alonso-Garcia et al., 2011; Barker et al., 2015; Margo_Project_Members, 2009; Wright & Flower, 2002]; Figure 6i), resulting in less enhancement of warm water transport into the Nordic Seas (relative to intermediate ice sheets) and a more accentuated increase in precipitation at lower latitudes with the AMOC in a strong mode. In fact, relative to the scenario with medium-sized ice sheets, we observe less precipitation right across the northern high-latitude land masses when ice sheets are at their maximum (LGM) size and the AMOC is strong (Figure 7h). We return to this point in Section 4.

3.4.2. Role of Atmospheric CO₂

It is likely that atmospheric CO₂ levels during post-MPT glacial maxima were lower than those prior to the MPT (Chalk et al., 2017; Hönlisch et al., 2009). Accordingly, it has been proposed that lower atmospheric CO₂ might have played a direct role in promoting the development of larger ice sheets across the MPT. To evaluate whether additional lowering of atmospheric CO₂ by ~35 ppm (Chalk et al., 2017; Hönlisch et al., 2009) could play a comparable role (as pre-existing NHIS sizes) in modulating NHIS surface mass balance, we utilized a published simulation (experiment NHIS_0.4s in Zhang et al., 2014) that was performed under the same ice-sheet configuration as IntICE_220 (Table S3) but with an LGM value of CO₂ (185 ppmv). We renamed this experiment “IntICE_185” in this study and ran it for another 800 years. Lowering CO₂ by 35 ppmv causes cooling (but without a significant change in the 0° summer surface temperature contour) and a decrease in precipitation (Figures S7 and S7b). Therefore, our experiment suggests that beginning with intermediate sized ice sheets, a lowering of CO₂ may actually cause a slowdown in the growth rate of northern ice sheets. In this respect, we agree with previous studies (Chalk et al., 2017; Hönlisch et al., 2009) which highlight the potential role of declining CO₂ as a feedback on the increasing severity of glacial periods across the MPT, rather than the trigger.

3.4.3. Role of Obliquity

As discussed, the development of longer glacial cycles across the MPT requires that the system be able to skip peaks in boreal summer insolation and in particular a peak related to high obliquity associated with IG 28. To test whether a pre-existing moderately sized NHIS bears the potential to survive this peak in summer insolation we conducted a high-obliquity experiment IntICE_Hobl_220. Comparison of SAT and Precip over NHIS regions between IntICE_Hobl_220 and IntICE_220 provides a qualitative estimation of the difference in NHIS surface mass balance. Our results show that higher obliquity has little effect on the 0°C isoline over the NHIS regions (Figure S7c) and hence will exert limited influence on the surface melting

Figure 7. Intermediate ice sheets benefit from stronger Atlantic Inflow, Earth system model (ESM) results show the effect of strengthening Atlantic Meridional Overturning Circulation (AMOC) (and Atlantic Inflow) under a range of ice sheet configurations (black contours represent topography in each case). In all cases, left hand panel shows 2 m temperature anomaly and right panel precipitation anomaly. Bright green line is the 0° summer temperature contour in strong AMOC mode (a, b) Strong minus weak AMOC for small (pre-industrial) ice sheets (c, d) same for intermediate (40% Last Glacial Maximum [LGM]) Northern hemisphere ice sheets (e, f) and large (LGM) ice sheets (g, h) difference between LGM and intermediate ice sheet configurations in strong AMOC mode (bright green line is 0° summer temperature contour for intermediate ice sheets, magenta line is zero-degree summer temperature contour for LGM ice sheets). Note that results are not corrected for lapse rate (topography) because we are interested in changes that occur at the elevation of the ice sheet surface.

rate of the NHIS. Additionally, precipitation decreases over the Laurentide ice sheet as obliquity increases (Figure S7d). These results therefore suggest that an intermediate-size NHIS could potentially survive a peak in summer insolation if the Nordic heat pump is strong, after which a decrease in obliquity would act to accelerate ice growth.

3.5. Possible Controls on the Nordic Heat Pump

Why should the Atlantic Inflow and Nordic heat pump have strengthened during interglacials over the past 1.2 Myr? One set of possibilities would see such an increase as a response to the increasing severity of glacial periods over this same period, that is, as a consequence of the MPT. Indeed, previous studies have noted a relationship between severe glacials and pronounced interglacials, provoking the idea that the strength of a glacial may influence the strength of the following interglacial (Lang & Wolff, 2011) and that intensifying glacial conditions during the MPT led to progressively more pronounced interglacial periods (Poirier & Billups, 2014). However, our results suggest that interglacial warming began prior to 1 Ma, well before the development of much larger ice sheets \sim 900 ka. We therefore suggest that strengthening of the Atlantic Inflow was the result of another factor, one more closely related to the actual cause of the MPT.

As illustrated by our climate model experiments, changes in the Atlantic Inflow could result from wider changes in the AMOC. Perhaps then we should be asking if and how the AMOC might have strengthened across the MPT? Raymo et al. (2006) hypothesized that the development of marine-based ice sheets around East Antarctica \sim 1 Ma gave rise to the apparent transition from \sim 41 to \sim 100 kyr periodicity of glacial cycles (the effect of precession having been canceled out by its out-of-phase effect in either hemisphere while Antarctic ice sheets were largely land based). Model results suggest that enlargement of the Antarctic ice sheet could lead directly to a strengthening of the AMOC (Shi et al., 2020). Moreover, recent evidence (Starr et al., 2021) suggests that iceberg calving around Antarctica may have increased from \sim 1.2 Ma, lending support to the idea that the Antarctic ice sheet increased its marine-based status at that time.

An alternative explanation for why the Atlantic Inflow may have strengthened over the past million years or so implicates variations in the depth of the Greenland-Scotland Ridge (GSR) as a function of the Iceland mantle plume. Building on earlier work (e.g., Vogt, 1972) Wright and Miller (1996) argued that changes in the flux of buoyant material within the Icelandic plume during the Neogene were responsible for altering the depth of the GSR and in turn the rate of deep water overflow across it. Since this overflow is an essential part of the Nordic heat pump they argued that changes in the buoyancy of the Icelandic Plume (which is related to its temperature) could have direct consequences for climate. Since then, several studies have provided various lines of evidence to support this contention (Poore et al., 2006, 2011; Parnell-Turner et al., 2014, 2015). These suggest that the Icelandic plume experienced a thermal minimum (meaning a deeper sill and increased exchange) between 5 and 3 Ma, which may explain why the high northern latitudes experienced such warm temperatures during the early Pliocene (Ravelo et al., 2004). Modeling studies provide physical support for such a scenario (Robinson et al., 2011; Starz et al., 2017). Subsequent warming of the plume occurred between 2.5 and 1.5 Ma and was paralleled by an inferred (Poore et al., 2006) decrease in NADW export (which might explain at least part of the cooling over that period). However, of direct relevance to this study is a subsequent switch from warming to a cooling of the plume since \sim 1.25 Ma and its acceleration toward temperatures more like those of the early Pliocene since \sim 0.5 Ma (Parnell-Turner et al., 2015). This could perhaps explain the mounting evidence for an increase in Atlantic Inflow since \sim 1.2 Ma (Baumann & Huber, 1999; Berger & Jansen, 1994; Henrich et al., 2002; Hernandez Almeida et al., 2012; Poirier & Billups, 2014; M. E. Raymo et al., 2004) with implications for the development of larger ice sheets across the MPT as we describe here.

4. Summary Discussion and Conclusions

We have shown that the transition from \sim 41 to \sim 100 kyr periodicity was diachronous across the NE Atlantic, providing a longer timescale analogy to the time transgressive cooling observed both at orbital (Alonso-Garcia et al., 2011; Wright & Flower, 2002) and millennial-timescales (Barker et al., 2015) in this region. In the case of the MPT, we suggest that such diachronicity reflected the increasing influence of expanding ice sheets (from the north) superimposed on the increasing transport of heat via the NAC (from the south).

We have argued (in line with several previous studies [e.g., Baumann & Huber, 1999; Berger & Jansen, 1994; Hernández Almeida et al., 2012; Poirier & Billups, 2014]) that a strengthening of Atlantic Inflow across the MPT played a role in the development of larger and longer lasting ice sheets since ~1 Ma. Our modeling results imply that strengthening Atlantic Inflow (at least as part of the wider AMOC) can have a positive or negative effect on ice sheet growth depending on the size of pre-existing ice sheets. Accordingly, we suggest that the interplay between gradual global cooling since the Pliocene (giving rise to medium-sized ice sheets of the 40 kyr world) and a strengthening Atlantic Inflow since ~1.2 Ma provided the impetus for the accelerated growth of ice sheets and their increasing ability to survive successive peaks in summer insolation across the MPT.

Of course, the positive effects of increased Atlantic Inflow apply only while the Atlantic Inflow is active. Our results therefore also suggest that the agent for producing larger ice sheets during the Late Pleistocene (i.e., a strong Atlantic Inflow) could also turn out to be their Achilles' heel, if the large size of LGM ice sheets actually limits their own high latitude moisture supply as the NAC becomes more zonal, then they could become susceptible to other sources of instability such as a rather modest increase in northern summer insolation. Perhaps this helps to explain why northern hemisphere ice sheets of the Late Pleistocene apparently become more susceptible to insolation forcing once they pass a critical threshold in size (Raymo, 1997). This paradox also highlights the peculiar nature of glacial terminations, when ice sheets continue to collapse even as the AMOC transitions to a strong mode. For example, sea level is thought to have risen by up to ~20 m during meltwater pulse 1 A, which coincided with the Bølling/Allerød interstadial during Termination 1 (Brendryen et al., 2020; Deschamps et al., 2012). At the same time, the AMOC and Atlantic Inflow are thought to have been strong during the B/A (McManus et al., 2004; Muller et al., 2009), which could explain the observed increase in snow accumulation over Greenland at that time (Alley et al., 1993). By definition, glacial terminations represent strongly nonlinear transitions (Barker & Knorr, 2021; Broecker & van Donk, 1970), involving the catastrophic collapse of large ice sheets (e.g., MacAyeal, 1979; Weertman, 1964), even if local accumulation rates are high. It seems that once the collapse of a large sheet has begun (after having reached its maximal glacial size) very little can be done to save it.

Any explanation for the MPT must account for the increasing size and longevity of northern continental ice sheets. If IG 28 (~995 ka) represents the first definitive time that northern ice sheets were able to survive a peak in summer insolation (that previously would have caused them to melt back fully to their interglacial extent), then the controlling mechanism must have been in play by that time. Changes occurring later must be considered consequences of the MPT rather than causes. Therefore, while our results cannot be used to rule out previous explanations for the increased duration and severity of glacial periods across the MPT they at least provide a minimum age (i.e., ~995 ka) for the responsible mechanism. Finally, we note that evidence from southwestern Norway and the northern North Sea region suggests that the first significant glaciation of Fenno-scandinavia (within the late Cenozoic) occurred around 1.1 Ma (Sejrup et al., 2000). Perhaps this was an earlier expression of a strengthening Atlantic Inflow that eventually gave rise to the MPT.

Conflict of Interest

The authors declare no perceived financial conflicts.

Data Availability Statement

Data produced in the study may be found in the Supplementary Material and online at the PANGAEA database (Barker, 2021a, 2012b; 2021c).

References

- Abelmann, A., Gersonde, R., Knorr, G., Zhang, X., Chaplignin, B., Maier, E., et al. (2015). The seasonal sea-ice zone in the glacial Southern Ocean as a carbon sink. *Nature Communications*, 6, 8136. <https://doi.org/10.1038/ncomms9136>
- Alley, R. B., Meese, D. A., Shuman, C. A., Gow, A. J., Taylor, K. C., Grootes, P. M., et al. (1993). Abrupt increase in Greenland snow accumulation at the end of the younger dryas event. *Nature*, 362, 527–529. <https://doi.org/10.1038/362527a0>
- Alonso-Garcia, M., Sierro, F. J., & Flores, J. A. (2011). Arctic front shifts in the subpolar North Atlantic during the mid-Pleistocene (800–400 ka) and their implications for ocean circulation. *Palaeogeography, Palaeoclimatology, Palaeoecology*, 311, 268–280. <https://doi.org/10.1016/j.palaeo.2011.09.004>

Acknowledgments

We acknowledge funding from the UK NERC (Grants NE/J008133/1, NE/P000878/1 and NE/L006405/1). This research used samples provided by the Integrated Ocean Drilling Program (IODP). We thank K-H. Baumann, M. Kucera, E. McClymont, R. Stratton, and P. Tzedakis for valuable discussions and advice. We also thank M. Hain and an anonymous reviewer for their valuable contribution. We thank Walter Hale, Holger Kuhlmann, and Alex Wülbers for assistance in sampling and curation.

- Atkins, E. D. (1991). *The evolution of Neogloboquadrina pachyderma (Ehrenberg) in the central Arctic Ocean and a comparison to its evolution in the North Atlantic Ocean*. University of Wisconsin-Madison.
- Austin, W. E. N., & Hibbert, F. D. (2012). Tracing time in the ocean: A brief review of chronological constraints (60–8 kyr) on North Atlantic marine event-based stratigraphies. *Quaternary Science Reviews*, 36, 28–37. <https://doi.org/10.1016/j.quascirev.2012.01.015>
- Bajo, P., Drysdale, R. N., Woodhead, J. D., Hellstrom, J. C., Hodell, D., Ferretti, P., et al. (2020). Persistent influence of obliquity on ice age terminations since the Middle Pleistocene transition. *Science*, 367, 1235–1239. <https://doi.org/10.1126/science.aaw1114>
- Barker, S. (2021a). *Faunal counts of planktonic foraminifera and sea surface temperatures from ODP site 983*. PANGAEA. <https://doi.org/10.1594/PANGAEA.929742>
- Barker, S. (2021b). *Planktic foraminiferal and ice rafted debris (IRD) counts from ODP site 983*. PANGAEA. <https://doi.org/10.1594/PANGAEA.929721>
- Barker, S. (2021c). *Planktic foraminiferal and ice rafted debris (IRD) counts from ODP site 981*. PANGAEA. <https://doi.org/10.1594/PANGAEA.929741>
- Barker, S., Chen, J., Gong, X., Jonkers, L., Knorr, G., & Thornalley, D. (2015). Icebergs not the trigger for North Atlantic cold events. *Nature*, 520, 333–336. <https://doi.org/10.1038/nature14330>
- Barker, S., & Knorr, G. (2021). Millennial scale feedbacks determine the shape and rapidity of glacial termination. *Nature Communications*, 12(1), 2273. <https://doi.org/10.1038/s41467-021-22388-6>
- Barker, S., Knorr, G., Conn, S., Lordsmith, S., Newman, D., & Thornalley, D. (2019). Early interglacial legacy of deglacial climate instability. *Paleoceanography and Paleoclimatology*, 34, 1455–1475. <https://doi.org/10.1029/2019PA003661>
- Baumann, K.-H., & Huber, R. (1999). Sea-surface gradients between the North Atlantic and the Norwegian Sea during the last 3.1 m.y.: Comparison of sites 982 and 985. *Proceedings of the Ocean Drilling Program, Scientific Results*, 162, 179–190.
- Bell, D. B., Jung, S. J. A., & Kroon, D. (2015). The Plio-Pleistocene development of Atlantic deep-water circulation and its influence on climate trends. *Quaternary Science Reviews*, 123, 265–282. <https://doi.org/10.1016/j.quascirev.2015.06.026>
- Berger, A., & Loutre, M. F. (1991). Insolation values for the climate of the last 10 million years. *Quaternary Science Reviews*, 10, 297–317. [https://doi.org/10.1016/0277-3791\(91\)90033-q](https://doi.org/10.1016/0277-3791(91)90033-q)
- Berger, W. H. (1968). Planktonic foraminifera: Selective solution and paleoclimatic interpretation. *Deep-Sea Research and Oceanographic Abstracts*, 15, 31–43. [https://doi.org/10.1016/0011-7471\(68\)90027-2](https://doi.org/10.1016/0011-7471(68)90027-2)
- Berger, W. H. (1970). Planktonic foraminifera: Selective solution and the lysocline. *Marine Geology*, 8, 111–138. [https://doi.org/10.1016/0025-3227\(70\)90001-0](https://doi.org/10.1016/0025-3227(70)90001-0)
- Berger, W. H., & Jansen, E. (1994). Mid-Pleistocene climate shift: The Nansen connection. In O. M. Johannessen, R. D. Muench, J. E. Overland (Eds.), *The polar oceans and their role in shaping the global environment* (pp. 295–311). American Geophysical Union.
- Bintanja, R., & Van de Wal, R. S. W. (2008). North American ice-sheet dynamics and the onset of 100,000-year glacial cycles. *Nature*, 454, 869–872. <https://doi.org/10.1038/nature07158>
- Boyer, T., Conkright, M., Levitus, S., Johnson, D., Antonov, J., O'Brien, T., et al. (1998). *World Ocean Database 1998 Volume 5: Temporal distribution of station data temperature and salinity profiles* (p. 108). Washington DC: US Gov Printing Office.
- Brendryen, J., Haflidason, H., Yokoyama, Y., Haaga, K. A., & Hannisdal, B. (2020). Eurasian ice sheet collapse was a major source of melt-water pulse 1A 14,600 years ago. *Nature Geoscience*, 13, 363–368. <https://doi.org/10.1038/s41561-020-0567-4>
- Broecker, W. S., & van Donk, J. (1970). Insolation changes, ice volumes, and the O¹⁸ in deep-sea cores. *Reviews of Geophysics*, 8, 169–198. <https://doi.org/10.1029/rg008i001p00169>
- Brovkin, V., Raddatz, T., Reick, C. H., Claussen, M., & Gayler, V. (2009). Global biogeophysical interactions between forest and climate. *Geophysical Research Letters*, 36. <https://doi.org/10.1029/2009GL037543>
- Chalk, T. B., Hain, M. P., Foster, G. L., Rohling, E. J., Sexton, P. F., Badger, M. P. S., et al. (2017). Causes of ice age intensification across the Mid-Pleistocene Transition. *Proceedings of the National Academy of Sciences of the United States of America*, 114, 13114–13119. <https://doi.org/10.1073/pnas.1702143114>
- Cheng, H., Edwards, R. L., Sinha, A., Spötl, C., Yi, L., Chen, S., et al. (2016). The Asian monsoon over the past 640,000 years and ice age terminations. *Nature*, 534, 640–646. <https://doi.org/10.1038/nature18591>
- Clark, P. U., Archer, D., Pollard, D., Blum, J. D., Rial, J. A., Brovkin, V., et al. (2006). The middle Pleistocene transition: Characteristics, mechanisms, and implications for long-term changes in atmospheric PCO₂. *Quaternary Science Reviews*, 25, 3150–3184. <https://doi.org/10.1016/j.quascirev.2006.07.008>
- Deschamps, P., Durand, N., Bard, E., Hamelin, B., Camoin, G., Thomas, A. L., et al. (2012). Ice-sheet collapse and sea-level rise at the Bølling warming 14,600 years ago. *Nature*, 483, 559–564. <https://doi.org/10.1038/nature10902>
- Dickson, R. R., & Brown, J. (1994). The production of North Atlantic Deep Water: Sources, rates, and pathways. *Journal of Geophysical Research*, 99, 12319–12341. <https://doi.org/10.1029/94jc00530>
- Dowsett, H. J., Cronin, T. M., Poore, R. Z., Thompson, R. S., Whatley, R. C., & Wood, A. M. (1992). Micropaleontological evidence for increased meridional heat transport in the North Atlantic Ocean during the Pliocene. *Science*, 258, 1133–1135. <https://doi.org/10.1126/science.258.5085.1133>
- Dowsett, H. J., Robinson, M., Haywood, A., Salzmann, U., Hill, D., Sohl, L., et al. (2010). The PRISM3D paleoenvironmental reconstruction. *Stratigraphy*, 7, 123–139.
- Elderfield, H., Ferretti, P., Greaves, M., Crowhurst, S., McCave, I. N., Hodell, D., & Piotrowski, A. M. (2012). Evolution of ocean temperature and ice volume through the Mid-Pleistocene climate transition. *Science*, 337, 704–709. <https://doi.org/10.1126/science.1221294>
- Eynaud, F. (2011). Planktonic foraminifera in the Arctic: Potentials and issues regarding modern and quaternary populations. *IOP Conference Series: Earth and Environmental Science*, 14(1), 012005. <https://doi.org/10.1088/1755-1315/14/1/012005>
- Farmer, J. R., Hönisch, B., Haynes, L. L., Kroon, D., Jung, S., Ford, H. L., et al. (2019). Deep Atlantic Ocean carbon storage and the rise of 100,000-year glacial cycles. *Nature Geoscience*, 12, 355–360. <https://doi.org/10.1038/s41561-019-0334-6>
- Frenz, M., Henrich, R., & Zychla, B. (2006). Carbonate preservation patterns at the Ceará Rise—Evidence for the Pliocene super conveyor. *Marine Geology*, 232, 173–180. <https://doi.org/10.1016/j.margeo.2006.07.006>
- Gong, X., Knorr, G., Lohmann, G., & Zhang, X. (2013). Dependence of abrupt Atlantic meridional ocean circulation changes on climate background states. *Geophysical Research Letters*, 40, 3698–3704. <https://doi.org/10.1002/grl.50701>
- Grinsted, A., Moore, J. C., & Jevrejeva, S. (2004). Application of the cross wavelet transform and wavelet coherence to geophysical time series. *Nonlinear Processes in Geophysics*, 11, 561–566. <https://doi.org/10.5194/npg-11-561-2004>
- Gu, S., Liu, Z., Jahn, A., Rempfer, J., Zhang, J., & Joos, F. (2019). Modeling neodymium isotopes in the ocean component of the community earth system model (CESM1). *Journal of Advances in Modeling Earth Systems*, 11, 624–640. <https://doi.org/10.1029/2018ms001538>

- Hansen, B., & Osterhus, S. (2000). North Atlantic-Nordic Seas exchanges. *Progress in Oceanography*, *45*, 109–208. [https://doi.org/10.1016/S0079-6611\(99\)00052-X](https://doi.org/10.1016/S0079-6611(99)00052-X)
- Hebbeln, D., Henrich, R., & Baumann, K. H. (1998). Paleoceanography of the last interglacial/glacial cycle in the Polar North Atlantic. *Quaternary Science Reviews*, *17*, 125–153. [https://doi.org/10.1016/S0277-3791\(97\)00067-X](https://doi.org/10.1016/S0277-3791(97)00067-X)
- Henrich, R., Baumann, K. H., Huber, R., & Meggers, H. (2002). Carbonate preservation records of the past 3 Myr in the Norwegian-Greenland Sea and the northern North Atlantic: Implications for the history of NADW production. *Marine Geology*, *184*(1–2), 17–39. [https://doi.org/10.1016/S0025-3227\(01\)00279-1](https://doi.org/10.1016/S0025-3227(01)00279-1)
- Hernández Almeida, I., Sierro, F. J., Flores, J. A., Cacho, I., & Filippelli, G. M. (2012). Palaeoceanographic changes in the North Atlantic during the Mid-Pleistocene Transition (MIS 31–19) as inferred from planktonic foraminiferal and calcium carbonate records. *Boreas*, *42*, 140–159. <https://doi.org/10.1111/j.1502-3885.2012.00283.x>
- Hibler, W. III (1979). A dynamic thermodynamic sea ice model. *Journal of Physical Oceanography*, *9*, 815–846. [https://doi.org/10.1175/1520-0485\(1979\)009<0815:adtsim>2.0.co;2](https://doi.org/10.1175/1520-0485(1979)009<0815:adtsim>2.0.co;2)
- Hodell, D., Lourens, L., Crowhurst, S., Konijnendijk, T., Tjallingii, R., Jiménez-Espejo, F., et al. (2015). A reference time scale for Site U1385 (Shackleton Site) on the SW Iberian Margin. *Global and Planetary Change*, *133*, 49–64. <https://doi.org/10.1016/j.gloplacha.2015.07.002>
- Hoffman, J. S., Clark, P. U., Parnell, A. C., & He, F. (2017). Regional and global sea-surface temperatures during the last interglaciation. *Science*, *355*, 276–279. <https://doi.org/10.1126/science.aai8464>
- Hönisch, B., Hemming, N. G., Archer, D., Siddall, M., & McManus, J. F. (2009). Atmospheric carbon dioxide concentration across the Mid-Pleistocene transition. *Science*, *324*, 1551–1554. <https://doi.org/10.1126/science.1171477>
- Hossain, A., Knorr, G., Lohmann, G., Stärr, M., & Jokat, W. (2020). Simulated thermohaline fingerprints in response to different Greenland-Scotland Ridge and Fram Strait subsidence histories. *Paleoceanography and Paleoclimatology*, *35*, e2019PA003842. <https://doi.org/10.1029/2019pa003842>
- Huber, R., Meggers, H., Baumann, K. H., Raymo, M. E., & Henrich, R. (2000). Shell size variation of the planktonic foraminifer *Neoglobobulimina papyroderma* in the Norwegian-Greenland Sea during the last 1.3 Myrs: Implications for paleoceanographic reconstructions. *Palaeogeography, Palaeoclimatology, Palaeoecology*, *160*, 193–212. [https://doi.org/10.1016/S0031-0182\(00\)00066-3](https://doi.org/10.1016/S0031-0182(00)00066-3)
- Hutson, W. H. (1979). The Agulhas Current during the Late Pleistocene: Analysis of modern faunal analogs. *Science*, *207*, 64–66.
- Huybers, P. (2011). Combined obliquity and precession pacing of late Pleistocene deglaciations. *Nature*, *480*, 229–232. <https://doi.org/10.1038/nature10626>
- Imbrie, J., Boyle, E. A., Clemens, S. C., Duffy, A., Howard, W. R., Kukla, G., et al. (1992). On the structure and origin of major glacial cycles 1. Linear responses to Milankovitch forcing. *Paleoceanography and Paleoclimatology*, *7*, 701–738. <https://doi.org/10.1029/92pa02253>
- Jansen, E., Raymo, M. E., & Blum, P. (1996). *Proceedings of the ocean drilling program initial reports*. OceanDrillingProgram, Texas A & M University.
- Juggins, S. (2017). *rioja: Analysis of Quaternary science data R package version 0.9-21*. <http://www.staff.ncl.ac.uk/stephen.juggins/>
- Jungclauss, J. H., Lorenz, S. J., Timmreck, C., Reick, C. H., Brovkin, V., Six, K., et al. (2010). Climate and carbon-cycle variability over the last millennium. *Climate of the Past*, *6*, 723–737. <https://doi.org/10.5194/cp-6-723-2010>
- Kim, J., Seguí, M. J., Yehudai, M., Knudson, K. P., Goldstein, S. L., Pena, L. D., & Ferretti, P. (2018). Reconstruction of the North Atlantic end-member of the Atlantic meridional overturning circulation over the last 2 Myr. *American Geophysical Union, fall meeting*. <https://doi.org/10.46427/gold2020.1306>
- Knies, J., Matthiessen, J., Vogt, C., Laberg, J. S., Hjelstuen, B. O., Smelror, M., et al. (2009). The Plio-Pleistocene glaciation of the Barents Sea-Svalbard region: A new model based on revised chronostratigraphy. *Quaternary Science Reviews*, *28*, 812–829. <https://doi.org/10.1016/j.quascirev.2008.12.002>
- Knorr, G., & Lohmann, G. (2014). Climate warming during Antarctic ice sheet expansion at the Middle Miocene transition. *Nature Geoscience*, *7*, 376–381. <https://doi.org/10.1038/ngeo2119>
- Kusu, C., Okada, M., Nozaki, A., Majima, R., & Wada, H. (2016). A record of the upper Olduvai geomagnetic polarity transition from a sediment core in southern Yokohama City, Pacific side of central Japan. *Progress in Earth and Planetary Science*, *3*, 1–13. <https://doi.org/10.1186/s40645-016-0104-7>
- Lambelet, M., van de Flierdt, T., Crocket, K., Rehkämper, M., Kreissig, K., Coles, B., et al. (2016). Neodymium isotopic composition and concentration in the western North Atlantic Ocean: Results from the GEOTRACES GA02 section. *Geochimica et Cosmochimica Acta*, *177*, 1–29. <https://doi.org/10.1016/j.gca.2015.12.019>
- Lang, N., & Wolff, E. W. (2011). Interglacial and glacial variability from the last 800 ka in marine, ice and terrestrial archives. *Climate of the Past*, *7*, 361. <https://doi.org/10.5194/cp-7-361-2011>
- Lawrence, K. T., Herbert, T. D., Brown, C. M., Raymo, M. E., & Haywood, A. M. (2009). High-amplitude variations in North Atlantic sea surface temperature during the early Pliocene warm period. *Paleoceanography and Paleoclimatology*, *24*. <https://doi.org/10.1029/2008pa001669>
- Lawrence, K. T., Sosdian, S., White, H., & Rosenthal, Y. (2010). North Atlantic climate evolution through the Plio-Pleistocene climate transitions. *Earth and Planetary Science Letters*, *300*, 329–342. <https://doi.org/10.1016/j.epsl.2010.10.013>
- Lear, C. H., Billups, K., Rickaby, R. E. M., Diester-Haass, L., Mawbey, E. M., & Sosdian, S. M. (2016). Breathing more deeply: Deep ocean carbon storage during the mid-Pleistocene climate transition. *Geology*, *44*, 1035–1038. <https://doi.org/10.1130/g38636.1>
- Lisiecki, L. E., & Raymo, M. E. (2005). A Pliocene-Pleistocene stack of 57 globally distributed benthic $\delta^{18}\text{O}$ records. *Paleoceanography and Paleoclimatology*, *20*. <https://doi.org/10.1029/2004PA001071>
- Locarnini, R. A., A. V. Mishonov, J. I. Antonov, T. P. Boyer, H. E. Garcia, O. K. Baranova, et al. (2010). World Ocean Atlas 2009, Volume 1: Temperature In S. Levitus (Ed.), *NOAA Atlas NESDIS* (p. 184). Washington DC: U.S. Government Printing Office.
- Lumpkin, R., & Johnson, G. C. (2013). Global ocean surface velocities from drifters: Mean, variance, El Niño-Southern Oscillation response, and seasonal cycle. *Journal of Geophysical Research*, *118*, 2992–3006. <https://doi.org/10.1002/jgrc.20210>
- MacAyeal, D. R. (1979). A catastrophe model of the paleoclimate. *Journal of Glaciology*, *24*, 245–257. <https://doi.org/10.3189/S0022143000014775>
- Maier, E., Zhang, X., Abelmann, A., Gersonde, R., Mulitza, S., Werner, M., et al. (2018). North Pacific freshwater events linked to changes in glacial ocean circulation. *Nature*, *559*, 241–245. <https://doi.org/10.1038/s41586-018-0276-y>
- Margo_Project_Members. (2009). Constraints on the magnitude and patterns of ocean cooling at the Last Glacial Maximum. *Nature Geoscience*, *2*, 127–132. <https://doi.org/10.1038/NGEO411>
- Marsland, S. J., Haak, H., Jungclauss, J. H., Latif, M., & Röske, F. (2003). The Max-Planck-Institute global ocean/sea ice model with orthogonal curvilinear coordinates. *Ocean Modelling*, *5*(2), 91–127. [https://doi.org/10.1016/S1463-5003\(02\)00015-X](https://doi.org/10.1016/S1463-5003(02)00015-X)

- McClymont, E. L., Rosell-Melé, A., Haug, G. H., & Lloyd, J. M. (2008). Expansion of subarctic water masses in the North Atlantic and Pacific oceans and implications for mid-Pleistocene ice sheet growth. *Paleoceanography and Paleoclimatology*, 23. <https://doi.org/10.1029/2008pa001622>
- McClymont, E. L., Sossian, S. M., Rosell-Melé, A., & Rosenthal, Y. (2013). Pleistocene sea-surface temperature evolution: Early cooling, delayed glacial intensification, and implications for the mid-Pleistocene climate transition. *Earth-Science Reviews*, 123, 173–193. <https://doi.org/10.1016/j.earscirev.2013.04.006>
- McManus, J. F., Francois, R., Gherardi, J.-M., Keigwin, L. D., & Brown-Leger, S. (2004). Collapse and rapid resumption of Atlantic meridional circulation linked to deglacial climate changes. *Nature*, 428, 834–837. <https://doi.org/10.1038/nature02494>
- McManus, J. F., Oppo, D. W., Keigwin, L. D., Cullen, J. L., & Bond, G. C. (2002). Thermohaline circulation and prolonged interglacial warmth in the North Atlantic. *Quaternary Research*, 58, 17–21. <https://doi.org/10.1006/qres.2002.2367>
- Meyers, S. R. (2014). *Astrochron: An R package for astrochronology*. <http://cran.r-project.org/package=astrochron>
- Milankovitch, M. (1941). *Kanon der Erdbestrahlung und seine Anwendung auf das Eiszeitenproblem* (p. 633). Royal Serbian Academy.
- Miller, K. G., Wright, J. D., Browning, J. V., Kulpecz, A., Komiz, M., Naish, T. R., et al. (2012). High tide of the warm Pliocene: Implications of global sea level for Antarctic deglaciation. *Geology*, 40, 407–410. <https://doi.org/10.1130/g32869.1>
- Mokeddem, Z., & McManus, J. F. (2016). Persistent climatic and oceanographic oscillations in the subpolar North Atlantic during the MIS 6 glaciation and MIS 5 interglacial. *Paleoceanography and Paleoclimatology*, 31, 758–778. <https://doi.org/10.1002/2015pa002813>
- Mokeddem, Z., McManus, J. F., & Oppo, D. W. (2014). Oceanographic dynamics and the end of the last interglacial in the subpolar North Atlantic. *Proceedings of the National Academy of Sciences*, 111, 11263–11268. <https://doi.org/10.1073/pnas.1322103111>
- Muller, J., Masse, G., Stein, R., & Belt, S. T. (2009). Variability of sea-ice conditions in the Fram Strait over the past 30,000 years. *Nature Geoscience*, 2, 772–776. <https://doi.org/10.1038/ngeo665>
- Ohkouchi, N., Eglinton, T. I., Keigwin, L. D., & Hayes, J. M. (2002). Spatial and temporal offsets between proxy records in a sediment drift. *Science*, 298(5596), 1224–1227. <https://doi.org/10.1126/science.1075287>
- Oppo, D. W., Keigwin, L. D., McManus, J. F., & Cullen, J. L. (2001). Persistent suborbital climate variability in marine isotope stage 5 and termination II. *Paleoceanography and Paleoclimatology*, 16, 280–292. <https://doi.org/10.1029/2000pa000527>
- Oppo, D. W., McManus, J. F., & Cullen, J. L. (1998). Abrupt climate events 500,000 to 340,000 years ago: Evidence from subpolar North Atlantic sediments. *Science*, 279, 1335–1338. <https://doi.org/10.1126/science.279.5355.1335>
- Østerhus, S., Woodgate, R., Valdimarsson, H., Turrell, B., de Steur, L., Quadfasel, D., et al. (2019). Arctic Mediterranean exchanges: A consistent volume budget and trends in transports from two decades of observations. *Ocean Science*, 15, 379–399. <https://doi.org/10.5194/os-15-379-2019>
- Otto-Bliesner, B. L., Jahn, A., Feng, R., Brady, E. C., Hu, A., & Löffverström, M. (2017). Amplified North Atlantic warming in the late Pliocene by changes in Arctic gateways. *Geophysical Research Letters*, 44, 957–964. <https://doi.org/10.1002/2016GL071805>
- Parnell-Turner, R., White, N., Henstock, T., Murton, B., MacLennan, J., & Jones, S. M. (2014). A continuous 55-million-year record of transient mantle plume activity beneath Iceland. *Nature Geoscience*, 7, 914–919. <https://doi.org/10.1038/ngeo2281>
- Parnell-Turner, R., White, N. J., McCave, I. N., Henstock, T. J., Murton, B., & Jones, S. M. (2015). Architecture of North Atlantic contourite drifts modified by transient circulation of the Icelandic mantle plume. *Geochemistry, Geophysics, Geosystems*, 16, 3414–3435. <https://doi.org/10.1002/2015GC005947>
- Pena, L. D., & Goldstein, S. L. (2014). Thermohaline circulation crisis and impacts during the mid-Pleistocene transition. *Science*, 345, 318–322. <https://doi.org/10.1126/science.1249770>
- Poirier, R. K., & Billups, K. (2014). The intensification of northern component deepwater formation during the mid-Pleistocene climate transition. *Paleoceanography and Paleoclimatology*, 29, 1046–1061. <https://doi.org/10.1002/2014pa002661>
- Poore, H., Samworth, R., White, N., Jones, S., & McCave, I. (2006). Neogene overflow of northern component water at the Greenland-Scotland Ridge. *Geochemistry, Geophysics, Geosystems*, 7. <https://doi.org/10.1029/2005gc001085>
- Poore, H., White, N., & MacLennan, J. (2011). Ocean circulation and mantle melting controlled by radial flow of hot pulses in the Iceland plume. *Nature Geoscience*, 4, 558–561. <https://doi.org/10.1038/ngeo1161>
- Prahl, F., Rontani, J., Zabeti, N., Walinsky, S. E., & Sparrow, M. A. (2010). Summer-biased sea-surface temperature record for alkenones in SE Alaskan surface sediments. *Geochimica et Cosmochimica Acta*, 74, 131–143. <https://doi.org/10.1016/j.gca.2009.09.027>
- R_Core_Team. (2020). *R: A language and Environment for statistical computing*. R Foundation for Statistical Computing. <https://www.R-project.org/>
- Ravelo, A. C., Andreasen, D. H., Lyle, M., Olivarez Lyle, A., & Wara, M. W. (2004). Regional climate shifts caused by gradual global cooling in the Pliocene epoch. *Nature*, 429, 263–267. <https://doi.org/10.1038/nature02567>
- Raymo, M. E. (1997). The timing of major climate terminations. *Paleoceanography and Paleoclimatology*, 12, 577–585. <https://doi.org/10.1029/97pa01169>
- Raymo, M. E., Grant, B., Horowitz, M., & Rau, G. H. (1996). Mid-Pliocene warmth: Stronger greenhouse and stronger conveyor. *Marine Micropaleontology*, 27, 313–326. [https://doi.org/10.1016/0377-8398\(95\)00048-8](https://doi.org/10.1016/0377-8398(95)00048-8)
- Raymo, M. E., Lisiecki, L. E., & Nisancioglu, K. H. (2006). Plio-Pleistocene ice volume, Antarctic Climate, and the global 180 record. *Science*, 313, 492–495. <https://doi.org/10.1126/science.1123296>
- Raymo, M. E., Oppo, D. W., Flower, B. P., Hodell, D. A., McManus, J. F., Venz, K. A., et al. (2004). Stability of North Atlantic water masses in face of pronounced climate variability during the Pleistocene. *Paleoceanography and Paleoclimatology*, 19, PA2008. <https://doi.org/10.1029/2003PA000921>
- Raymo, M., Ruddiman, W., & Clement, B. (1987). Pliocene-Pleistocene paleoceanography of the North-Atlantic at deep-sea drilling project site-609. *Initial Reports of the Deep Sea Drilling Project*, 94, 895–901.
- Robinson, M. M., Valdes, P. J., Haywood, A. M., Dowsett, H. J., Hill, D. J., & Jones, S. M. (2011). Bathymetric controls on Pliocene North Atlantic and Arctic sea surface temperature and deepwater production. *Palaeogeography, Palaeoclimatology, Palaeoecology*, 309, 92–97. <https://doi.org/10.1016/j.palaeo.2011.01.004>
- Rodrigues, T., Alonso-Garcia, M., Hodell, D. A., Rufino, M., Naughton, F., Grimalt, J. O., et al. (2017). A 1-Ma record of sea surface temperature and extreme cooling events in the North Atlantic: A perspective from the Iberian Margin. *Quaternary Science Reviews*, 172, 118–130. <https://doi.org/10.1016/j.quascirev.2017.07.004>
- Roeckner, E., Bäuml, G., Bonventura, L., Brokopf, R., Esch, M., Giorgetta, M., et al. (2003). *The atmospheric general circulation model ECHAM5. PART I: Model description report 349*. Max Planck Institute for Meteorology.
- Ruddiman, W. F., & McIntyre, A. (1979). Warmth of the Subpolar North Atlantic Ocean during Northern Hemisphere ice-sheet growth. *Science*, 204, 173–175. <https://doi.org/10.1126/science.204.4389.173>

- Ruddiman, W. F., McIntyre, A., & Raymo, M. (1987). Paleoenvironmental Results from North-Atlantic site-607 and site-609. *Initial Reports of the Deep Sea Drilling Project*, 94, 855–878.
- Schlitzer, R. (2018). *Ocean Data View*. <http://odv.awi.de>
- Sejrup, H. P., Larsen, E., Landvik, J., King, E. L., Hafliðason, H., & Nesje, A. (2000). Quaternary glaciations in southern Fennoscandia: evidence from southwestern Norway and the northern North Sea region. *Quaternary Science Reviews*, 19(7), 667–685. [https://doi.org/10.1016/S0277-3791\(99\)00016-5](https://doi.org/10.1016/S0277-3791(99)00016-5)
- Seki, O., Foster, G. L., Schmidt, D. N., Mackensen, A., Kawamura, K., & Pancost, R. D. (2010). Alkenone and boron-based Pliocene pCO₂ records. *Earth and Planetary Science Letters*, 292, 201–211. <https://doi.org/10.1016/j.epsl.2010.01.037>
- Shi, F., Yin, Q., Nikolova, I., Berger, A., Ramstein, G., & Guo, Z. (2020). Impacts of extremely asymmetrical polar ice sheets on the East Asian summer monsoon during the MIS-13 interglacial. *Quaternary Science Reviews*, 230, 106164. <https://doi.org/10.1016/j.quascirev.2020.106164>
- Shimada, C., Sato, T., Toyoshima, S., Yamasaki, M., & Tanimura, Y. (2008). Paleocological significance of laminated diatomaceous oozes during the middle-to-late Pleistocene, North Atlantic Ocean (IODP Site U1304). *Marine Micropaleontology*, 69, 139–150. <https://doi.org/10.1016/j.marmicro.2008.07.004>
- Siccha, M., & Kucera, M. (2017). ForCenS, a curated database of planktonic foraminifera census counts in marine surface sediment samples. *Scientific Data*, 4, 170109. <https://doi.org/10.1038/sdata.2017.109>
- Starr, A., Hall, I. R., Hall, I. R., Barker, S., Rackow, T., Zhang, X., et al. (2021). Antarctic icebergs reorganize ocean circulation during Pleistocene glacials. *Nature*, 589, 236–241. <https://doi.org/10.1038/s41586-020-03094-7>
- Stärz, M., Jokat, W., Knorr, G., & Lohmann, G. (2017). Threshold in North Atlantic-Arctic Ocean circulation controlled by the subsidence of the Greenland-Scotland Ridge. *Nature Communications*, 8. <https://doi.org/10.1038/ncomms15681>
- Stepanek, C., Samakinwa, E., Knorr, G., & Lohmann, G. (2020). Contribution of the coupled atmosphere-ocean-sea ice-vegetation model COSMOS to the PlioMIP2. *Climate of the Past*, 16, 2275–2323. <https://doi.org/10.5194/cp-16-2275-2020>
- Telford, R., & Birks, H. (2009). Evaluation of transfer functions in spatially structured environments. *Quaternary Science Reviews*, 28, 1309–1316. <https://doi.org/10.1016/j.quascirev.2008.12.020>
- Trachsel, M., & Telford, R. J. (2016). Technical note: Estimating unbiased transfer-function performances in spatially structured environments. *Climate of the Past*, 12, 1215–1223. <https://doi.org/10.5194/cp-12-1215-2016>
- Tzedakis, P. C., Crucifix, M., Mitsui, T., & Wolff, E. W. (2017). A simple rule to determine which insolation cycles lead to interglacials. *Nature*, 542, 427–432. <https://doi.org/10.1038/nature21364>
- Vogt, P. R. (1972). The Faeroe-Iceland-Greenland aseismic ridge and the western boundary undercurrent. *Nature*, 239, 79–81. <https://doi.org/10.1038/239079a0>
- Weertman, J. (1964). Rate of growth or shrinkage of nonequilibrium ice sheets. *Journal of Glaciology*, 5, 145–158. <https://doi.org/10.3189/s0022143000028744>
- Wei, W., & Lohmann, G. (2012). Simulated Atlantic multidecadal oscillation during the Holocene. *Journal of Climate*, 25, 6989–7002. <https://doi.org/10.1175/jcli-d-11-00667.1>
- Wei, W., Lohmann, G., & Dima, M. (2012). Distinct modes of internal variability in the global meridional overturning circulation associated with the Southern Hemisphere westerly winds. *Journal of Physical Oceanography*, 42, 785–801. <https://doi.org/10.1175/jpo-d-11-038.1>
- Willeit, M., Ganopolski, A., Calov, R., & Brovkin, V. (2019). Mid-Pleistocene transition in glacial cycles explained by declining CO₂ and regolith removal. *Science Advances*, 5, eaav7337. <https://doi.org/10.1126/sciadv.aav7337>
- Wright, A. K., and B. P. Flower, (2002). Surface and deep ocean circulation in the subpolar North Atlantic during the mid-Pleistocene revolution. *Paleoceanography and Paleoclimatology*, 17, 1068. <https://doi.org/10.1029/2002pa000782>
- Wright, J. D., & Miller, K. G. (1996). Control of North Atlantic deep water circulation by the Greenland-Scotland Ridge. *Paleoceanography and Paleoclimatology*, 11, 157–170. <https://doi.org/10.1029/95pa03696>
- Zhang, X., Knorr, G., Lohmann, G., & Barker, S. (2017). Abrupt North Atlantic circulation changes in response to gradual CO₂ forcing in a glacial climate state. *Nature Geoscience*, 10, 518–523. <https://doi.org/10.1038/ngeo2974>
- Zhang, X., Lohmann, G., Knorr, G., & Purcell, C. (2014). Abrupt glacial climate shifts controlled by ice sheet changes. *Nature*, 512, 290–294. <https://doi.org/10.1038/nature13592>
- Zhang, X., Lohmann, G., Knorr, G., & Xu, X. (2013). Different ocean states and transient characteristics in Last Glacial Maximum simulations and implications for deglaciation. *Climate of the Past*, 9, 2319–2333. <https://doi.org/10.5194/cp-9-2319-2013>